6-2023

Fully Coupled Fluid Structure Interaction Simulation of Bioprosthetic Heart Valves: A Numerical and Experimental Analysis

Masod Sadipour

Fully Coupled Fluid Structure Interaction Simulation of Bioprosthetic Heart Valves: A Numerical and Experimental Analysis

Abstract

Aortic stenosis impacts approximately 7% of the global population. In the past decade, the role of computational modeling has been becoming considerably important in the design of BHVs. To obtain reliable solutions in computational modeling, it is essential to consider accurate properties of bioprosthetic heart valves (BHVs), such as density and mechanical properties. Previous computational studies assumed (bovine pericardium) BP used in BHVs density was comparable to water or blood. Yet, BP is subjected to multiple treatments like fixation and anti-calcification. In Chapter 2, I measured BP density and its effect on BHV leaflet stress and strain. In the second study, Chapter 3, I've developed a new framework to investigate the bioprosthetic heart valve (BHV) interaction with the blood flow passing through the valve inside a pulse duplicator system. This project is a major step towards the experimental validation of FSI modeling for analyzing tissue heart valves.

Document Type

Masters Thesis

Degree Name

M.S.

First Advisor

Ali Azadani

Second Advisor

Matt Gordon

Third Advisor

Laleh Mehran

Keywords

Cardiovascular mechanics, Data analysis, Fluid structure analysis, Heart valves, Hemodynamics, Numerical analysis

Subject Categories

Biomechanical Engineering | Biomedical Devices and Instrumentation | Biomedical Engineering and Bioengineering | Engineering | Mechanical Engineering

Fully Coupled Fluid Structure Interaction Simulation of Bioprosthetic Heart Valves: A Numerical and Experimental Analysis

A Thesis

Presented to

the Faculty of the Daniel Felix Ritchie School of Engineering and Computer Science

University of Denver

_____

In Partial Fulfillment

of the Requirements for the Degree

Master of Science

_____

by

Masod Sadipour

June 2023

Advisor: Dr. Ali Azadani

Author: Masod Sadipour
Title: Fully Coupled Fluid Structure Interaction Simulation of Bioprosthetic Heart Valves: A Numerical and Experimental Analysis
Advisor: Dr. Ali Azadani
Degree Date: June 2023

ABSTRACT

Aortic stenosis impacts approximately 7% of the global population. In the past decade, the role of computational modeling has been becoming considerably important in the design of BHVs. To obtain reliable solutions in computational modeling, it is essential to consider accurate properties of bioprosthetic heart valves (BHVs), such as density and mechanical properties. Previous computational studies assumed (bovine pericardium) BP used in BHVs density was comparable to water or blood. Yet, BP is subjected to multiple treatments like fixation and anti-calcification. In Chapter 2, I measured BP density and its effect on BHV leaflet stress and strain. In the second study, Chapter 3, I've developed a new framework to investigate the bioprosthetic heart valve (BHV) interaction with the blood flow passing through the valve inside a pulse duplicator system. This project is a major step towards the experimental validation of FSI modeling for analyzing tissue heart valves.

TABLE OF CONTENTS

LIST OF TABLES

LIST OF FIGURES

CHAPTER ONE: INTRODUCTION

1.1. Human Cardiovascular System Anatomy and Physiology

The cardiovascular system in the human body is responsible for supplying blood to the organs through the process of circulation [1]. The circulatory system transports blood throughout the body via blood vessels, including arteries, veins, and capillaries, to deliver oxygen, nutrients, and other substances to the tissues of the body, and remove waste products such as carbon dioxide.

The functions of the cardiovascular system can be summarized as follows [2]:

1. Oxygen supply to tissues.
2. Providing the nutrients needed by the cells in the tissues.
3. Excreting CO_2 and other waste materials from the body.
4. Regulation of body temperature.

The cardiovascular system comprises the heart, blood vessels (such as veins, arteries, and capillaries), and blood. The heart, a muscular organ, propels blood throughout the body, while the blood vessels serve as conduits for blood flow. The blood consists of red blood cells, white blood cells, plasma, and platelets.

To achieve its functions, the cardiovascular system is divided into three main circuits or subsets:

1. Systemic circulation
2. Pulmonary circulation
3. Coronary circulation

In systemic circulation, oxygen-rich blood is pumped from the left ventricle of the heart into the aorta. The aorta branches into smaller arteries that Transport blood filled with oxygen to the body's tissues and organs. The capillaries within the tissues allow for the transfer of oxygen and nutrients from the blood to the body's cells, and the removal of CO2 and waste products from cells and carries them away for elimination. The oxygen poor blood then flows back to the heart through the veins, which eventually join to form the superior and inferior vena cava, the two largest veins in the body. These veins return the oxygen-poor blood to the heart's right atrium, completing the systemic circulation[2]. During pulmonary circulation, the heart pumps deoxygenated blood from the right ventricle into the pulmonary artery, which transports it to the lungs. In the lungs, the blood undergoes gas exchange, where it takes up oxygen and releases carbon dioxide. Afterward, the oxygenated blood flows back to the heart through the pulmonary veins, which empty into the left atrium. The left ventricle then pumps the oxygen-rich blood to the aorta to start systemic circulation again [3]. Figure 1-1 shows a schematic view of blood circulation system.

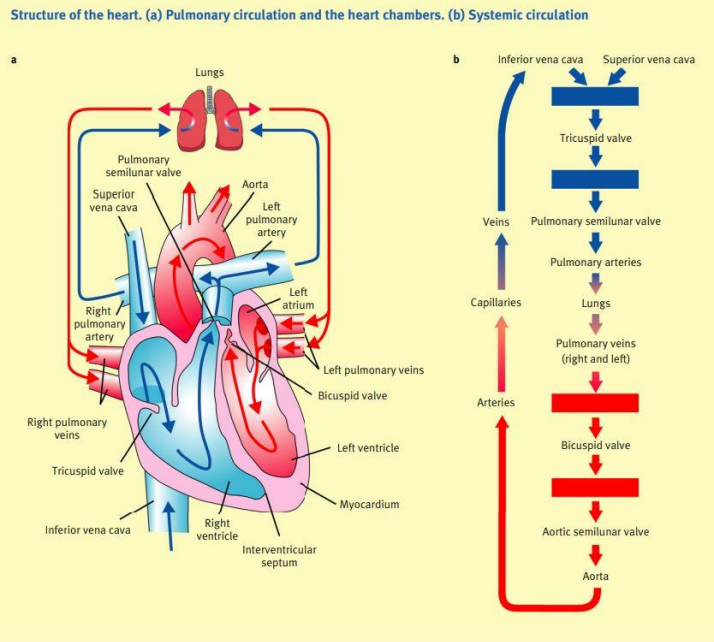

Figure 1- 1-Schematic view of the blood circulation system [4].

Coronary circulation refers to the circulation of blood within the heart muscle itself. For the heart muscle or myocardium to function adequately, it necessitates a continuous supply of oxygen and nutrients. The coronary circulation supplies this oxygen and nutrient-rich blood to the heart muscle [4].

1.2. Heart Valves

The heart has four valves that help regulate blood flow through the heart and to the rest of the body. Blood valves play a crucial role in maintaining one-way blood flow in the heart. The complex structure of these valves has evolved to withstand billions of cycles during their lifetime. From a mechanical engineering standpoint, these valves are remarkably durable and efficient.

These valves are:

1. Tricuspid valve: The tricuspid valve, positioned between the right atrium and right ventricle, consists of three cusps that regulate the flow of blood from the atrium to the ventricle by opening and closing and also prevent backflow.
2. Pulmonary valve: It's situated between the right ventricle and pulmonary artery, comprises three cusps that permit blood flow from the heart to the lungs and prevent the reverse flow.
3. Mitral valve: It is situated between the left atrium and left ventricle, comprises two cusps that open and close to permit blood to move from the atrium to the ventricle and prevent backflow.
4. Aortic valve: It's located between the left ventricle and the aorta, comprises three cusps that open and close to permit blood to move from the heart to the rest of the body and prevent backflow.

The opening and closing of the valves are triggered by the variations in the pressure and volume of the heart chambers. When the heart contracts, the aorta and pulmonary valves open to allow blood to be distributed to the rest of the body and lungs, and when the heart relaxes, the mentioned valves close to prevent backflow [5].

As a result of fluid-solid interaction between pulsatile blood flow and heart valve leaflets, these valves are continuously loaded during a cardiac cycle. These loads include compression, stretching and bending. These mechanical stresses affect the cells of the inner lining of the same endothelial. Mechanical stresses, along with genetic and environmental factors, can activate a series of biochemical reactions that ultimately lead to tissue changes. It can lead to unhealthy congenital formation of valve leaflets [1] and valve occlusion. Genetic and environmental factors can cause calcification of the aorta, bicuspid aortic valve disease [2], and aggravate the hemodynamic changes of the flow in the ascending aorta, phenomena that are considered as one of the main factors in the swelling of the ascending aorta.

Valvular heart disease is a widespread condition that affects over 100 million people globally and can lead to significant mortality rates in severe cases [6]. With the aging population, the number of patients suffering from heart diseases is on the rise worldwide [1,7,8] Common issues associated with the aortic valve include valve calcification, valve stiffening, rheumatic fever, and congenital bicuspid valve. Heart valve problems leading to conditions such as regurgitation (backflow of blood) or stenosis (narrowing of the valve opening). These conditions can result in symptoms such as fatigue, chest pain, and shortness of breath. Treatment for heart valve disease depends on the severity of the condition and the symptoms experienced. The treatment for aortic valve disease depends on various factors such as the severity of the condition, presence of symptoms, and the rate of disease progression. The treatment plan can include monitoring, lifestyle modifications, medications, surgical procedures, or other interventions. Surgery or catheter-based procedures may be necessary to repair or replace the damaged aortic valve. In some cases, surgery may be required even if the condition is not severe, or symptoms are not present. The surgical approach may involve open-heart surgery, during which the surgeon may separate fused valve flaps, add support to the base of the valve, reshape or remove excess valve tissue, or patch holes or tears in the valve. Valve replacement may also be necessary, involving the removal of the damaged valve and replacing it with a prosthetic valve made of either biological or mechanical materials. This can be achieved through minimally

invasive heart surgery or catheter-based procedures. For children with aortic valve stenosis, balloon valvuloplasty may be used to temporarily widen the narrowed valve. This procedure involves inserting a catheter into a blood vessel and inflating a balloon to expand the valve opening. It may also be considered for adults who are not candidates for surgery or awaiting valve replacement[9].

1.3. Artificial Heart Valves

Prosthetic heart valves are devices used to replace damaged or diseased heart valves. There are several different types of artificial heart valves, each with its own advantages and disadvantages. Here are the three main types of artificial heart valves:

1. Mechanical Heart Valves: Mechanical heart valves are made from materials such as metal or carbon. They are very long-lasting and can last for several decades. However, patients with mechanical heart valves require lifelong anticoagulation therapy to prevent blood clots from forming on the valve.

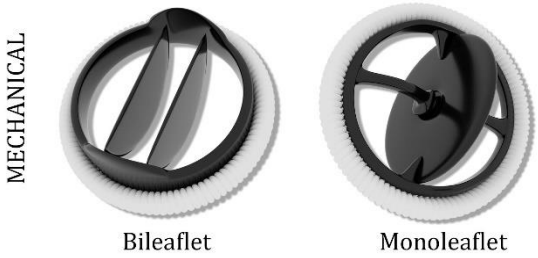

Figure 1- 2-Mechanical heart valves, bileaflet and monoleaflet [10].

2. Bioprosthetic Heart Valves: Biological heart valves are made from animal tissue, such as cow or pig heart tissue. They are less durable than mechanical valves but do not require lifelong anticoagulation therapy. They are often used in older patients who are not good candidates for mechanical valves.

2.1- Surgical Aortic Valve Replacement (SAVR):

SAVR is commonly used to treat patients with severe aortic stenosis. This procedure involves the removal of the damaged aortic valve and replacement with tissue

valves. Bioprosthetic heart valve (BHV) replacements are preferred for patients who cannot take blood thinners or are under 60 years old. Bioprosthetic valves are made using animal tissues such as cow or pig pericardium. The tissues are chemically treated with glutaraldehyde and then sewn onto a metal frame to imitate the natural one-way flow of heart valve leaflets by sealing against each other. Fig. 1.3 illustrates examples of stented and stentless bioprosthetic surgical valves. Surgical bioprosthetic aortic valves (SAVs) are known for their excellent biocompatibility and hemodynamic performance. Among the commercially available BHVs, the Carpentier-Edwards PERIMOUNT pericardial bioprosthesis is a reliable choice for SAVR due to its low rate of structural valve deterioration at 20 years [11].

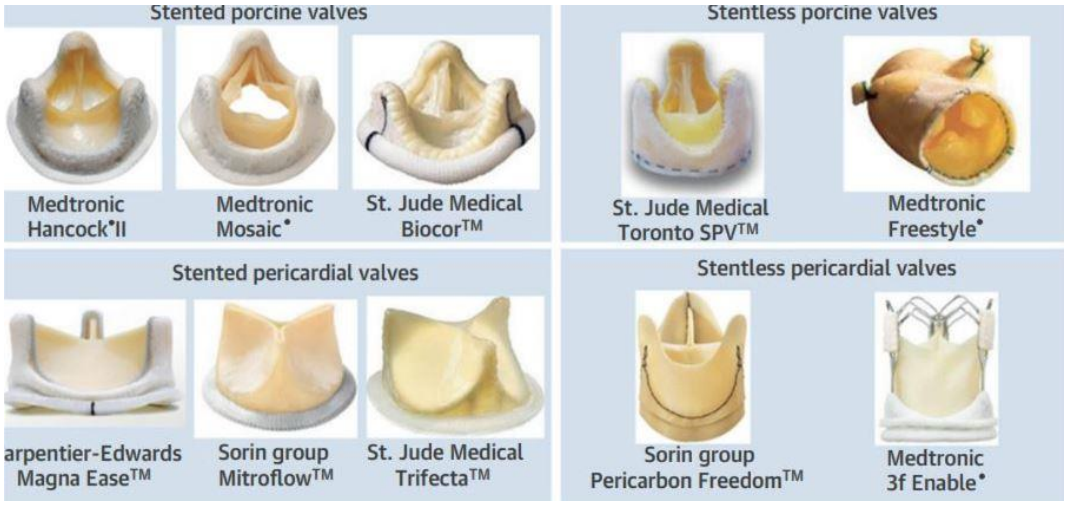

Figure 1- 3-Bioprosthetic heart valves[10].

2.2- Transcatheter Aortic Valve Replacement:

Transcatheter heart valves are a newer type of heart valve that can be inserted into the heart through a small incision in the leg or chest. They can be used for high-, moderate, and low-risk patients with aortic stenosis. Transcatheter valves can be classified into two main types based on their implantation location: balloon expanded valves and self-expandable valves. These can also be further divided into two categories based on their design: intra-annular and supra-annular. Intra-annular valves are designed to sit inside the native valve annulus, whereas supra-annular valves are positioned above the annulus.

Supra-annular valves may provide a larger effective orifice area, allowing for improved blood flow and reduced pressure gradients across the valve. Some of the commonly used TAVs include the balloon-expandable Edwards SAPIEN and SAPIEN XT valves, the self-expandable CoreValve and Evolut R valves, and the Lotus valve, which is a mechanically expanding valve [12].

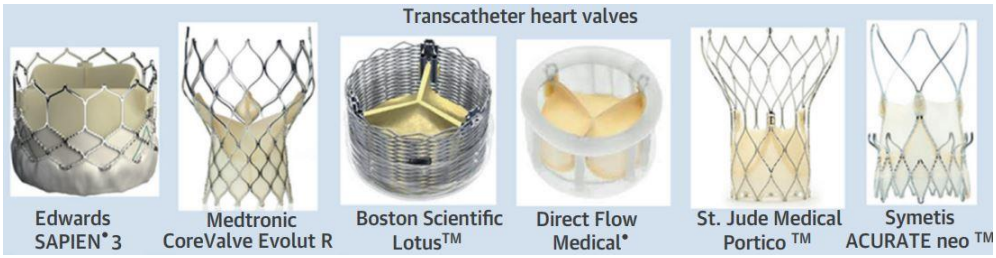

Figure 1- 4-Transcatheter heart valves [10].

3. Tissue-Engineered Heart Valves:

Researchers are developing bioartificial heart valves with a patient's own cells using tissue engineering methods. Synthetic or natural polymer scaffolds are seeded with differentiated, progenitor or stem cells and cultivated in specialized bioreactors. This approach aims to create durable, biocompatible heart valves with appropriate mechanical properties that can grow with a child. Recent studies show promising results with nanostructured scaffolds. They have the potential to last longer than biological valves and do not require anticoagulation therapy. However, they are not widely available and are still being developed and tested [13–15].

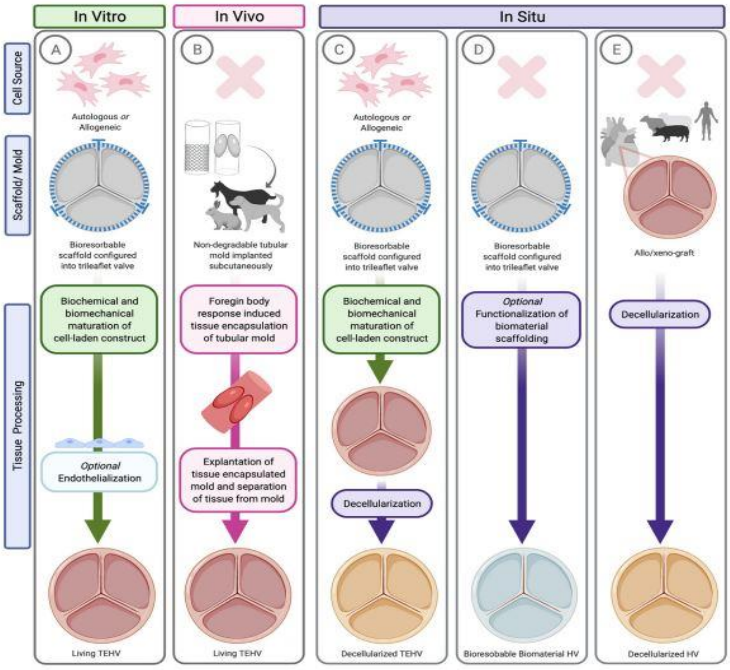

Figure 1- 5-Tissue-engineered heart valves[15].

1.4. BHVs Complications: Long Term Durability and Thrombosis

Biological heart valves (BHV) are a common type of heart valve used to replace damaged or diseased heart valves. While BHVs are generally well-tolerated, there are some potential complications associated with their use. Some of the most common complications include:

1. Structural valve deterioration: Over time, BHVs can become worn or damaged, leading to decreased valve function and the need for replacement.

   The long-term durability of biological heart valves (BHV) is an important consideration when deciding on a replacement valve for patients with heart valve disease. BHVs are made from animal tissue, either from pigs, cows or human donors, and their durability can vary depending on several factors. One of the main factors affecting BHV durability is the type of tissue used to create the valve, but all biological valves will eventually wear out over time. The durability of BHVs can also be affected by factors such as patient age, activity level, and overall health. While BHVs are generally not as durable as mechanical valves, they have several

advantages, including a lower risk of blood clots and a decreased need for anticoagulation therapy. The durability of BHVs can be improved by using newer, more advanced tissue processing techniques, which can reduce the risk of structural valve deterioration and prolong the life of the valve. Overall, the long-term durability of BHVs is an important consideration when deciding on a replacement valve for patients with heart valve disease. The doctor or cardiologist can help the one to understand the risks and benefits of BHV replacement and determine the best course of treatment for the individual needs. Regular follow-up with your healthcare team is also important to monitor the function of the BHV over time and identify any potential complications early.

Figure 1- 6- Classification of valves[16].

2. Valve thrombosis: Although BHVs do not require anticoagulation therapy like mechanical valves, there is still a risk of blood clots forming on the valve, which can lead to stroke or other serious complications [17]. Thrombosis is a condition where a blood clot forms inside a blood vessel or on the surface of a medical device such as a heart valve. Thrombosis of biological heart valves (BHV) is a rare but serious complication that can occur after valve replacement surgery. BHV thrombosis occurs when blood clots form on or around the valve leaflets, obstructing blood flow through the valve. This can lead to symptoms such as chest pain, shortness of breath, and fatigue. In severe cases, BHV thrombosis can cause heart failure or stroke.

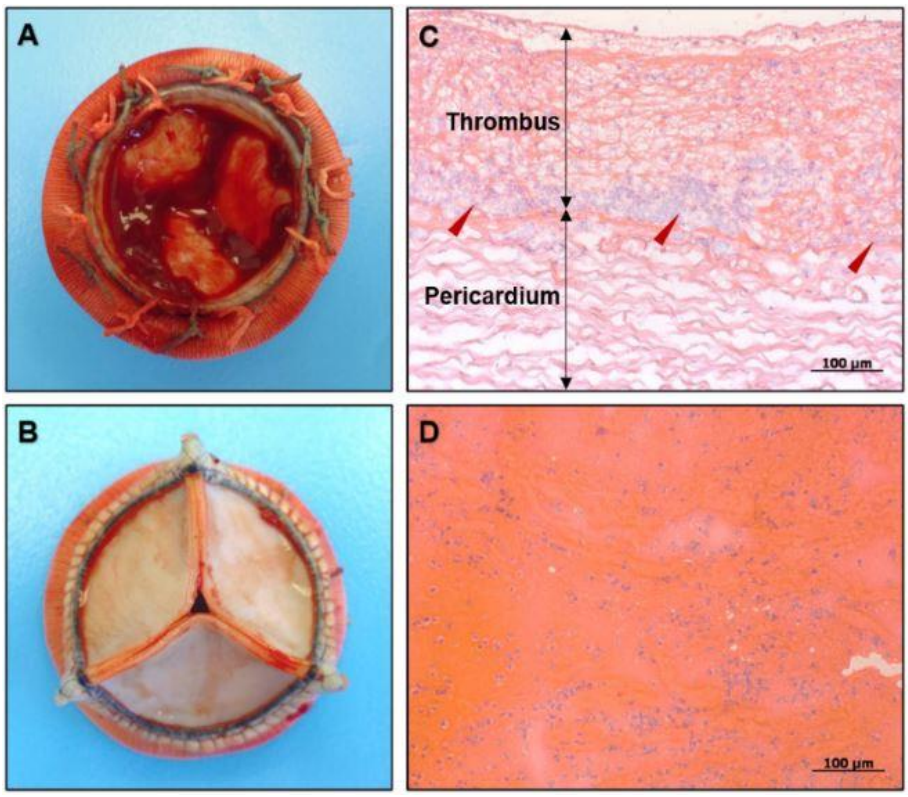

Figure 1- 7- Comprehensive examination of the excised bioprosthetic valve (A) A large thrombus was found on the side where the valve takes in blood; (B) The other side of the valve, where blood flows out, did not have any blood clot formation; (C) The blood clot was heavily infiltrated by polymorphonuclear leukocytes (indicated by red arrows) at the top, but these cells did not invade the artificial leaflets at the bottom. This was observed through the use of hematoxylin and eosin staining, at a magnification of ×200. The scale bar represents 100 µm; (D) The thrombus in the left atrium also contained a significant number of polymorphonuclear leukocytes. This was visualized using hematoxylin and eosin staining, at a magnification of ×200. The scale bar represents 100 µm [18].

The risk of BHV thrombosis is lower than the risk of thrombosis with mechanical heart valves, as BHVs do not require anticoagulation therapy. However, BHV thrombosis can still occur in some patients, particularly those with underlying medical conditions or risk factors for blood clotting. Treatment of BHV thrombosis typically involves anticoagulation therapy with medications such as warfarin to prevent further blood clots from forming. In some cases, surgery may be necessary to remove the clot or replace the valve [17]. Prevention of BHV thrombosis involves careful monitoring of the patient's

condition and regular follow-up with their healthcare team. Patients with BHVs should also be advised to seek medical attention if they experience symptoms of thrombosis, such as chest pain or shortness of breath.

In summary, thrombosis of BHVs is a rare but serious complication that can occur after valve replacement surgery. While the risk of BHV thrombosis is lower than with mechanical heart valves, it is still a potential concern for some patients. The doctor or cardiologist can help understand the risks and benefits of BHV replacement and determine the best course of treatment for the individual needs.

1.5. Computational Modeling

The creation and advancement of implantable medical devices, like heart valves, currently necessitate costly and extensive preclinical and clinical evaluations under the existing regulatory framework. This procedure restricts the chances to improve existing designs and investigate new, daring concepts [19]. However, in recent years, computational modeling has become considerably important in the design and validation of medical equipment. The significance of computational modeling is growing in the design and validation of medical equipment. It furnishes a numerical structure for explaining device performance and delivers higher uniformity and forecastability while developing new devices. Furthermore, computational modeling has the potential to generate substantial cost savings by decreasing the necessity for laborious pre-clinical animal experiments. Consequently, Computational modeling and simulations have become a crucial part of research and development in the medical equipment sector, prompted in some measure by the regulatory obligations of the U.S. Food and Drug Administration (FDA) and CE Mark[20].

1.5.1. Finite Element Analysis

Several studies have primarily focused on using finite element (FE) methods to mechanically model the valve while neglecting the valve and blood flow interaction. For example, references [21,22] , among others, have primarily focused on FE-based static

analyses of the valve in the fully closed position [25–29]. To better understand the dynamic behavior of bioprosthetic heart valves (BHV), researchers have also conducted analyses by utilizing physiological pressure loads that change over time to calculate how flexible leaflets deform and how stress is distributed throughout the cardiac cycle [21,23–25]. For instance, Lim et al. [24] employed a linear isotropic material model for the mitral valve to investigate the impact of asymmetry. However, Patterson et al. [23] have emphasized the significance of including non-linear (isotropic) constitutive models since they demonstrate more intricate deformations and increased stress levels in the presence of time-varying pressure circumstances. Kunzelman et al. [26] Created a dynamic finite element (FE) model utilizing linear anisotropic material characteristics for the mitral valve and employed it to examine the consequences of collagen concentration and leaflet thickness [27]. They emphasize the fact that the aortic valve leaflets and roots possess anisotropic qualities, which is also supported by De Hart et al. [22]. Therefore, it is important to consider both anisotropic and non-linear characteristics in FE analyses of bioprosthetic heart valves (BHV).

Kim et al. [25][28] have utilized the Finite Element Analysis Program (FEA P) to establish a dynamic finite element (FE) model incorporating a non-linear anisotropic Fung-type elastic constitutive model for pericardial bioprosthetic heart valve (BHV). Hammer et al. [29] created a mass-spring model to replicate a bioprosthetic heart valve (BHV) and evaluated it against a dynamic finite element (FE) model that incorporates a non-linear anisotropic Fung-type constitutive law for BHs, founded on the FE formulation described in [30]. Although the mass-spring model being quicker, it had lower accuracy in capturing the non-linear and anisotropic behavior of the tissue.

1.5.2. Material Characterization Using Optimization

It is important to take into account the mechanical characteristics of biological soft tissue in order to create a dependable computational model. For the purpose of this research, a surgical bioprosthetic heart valve known as the Carpentier-Edwards PERIMOUNT Magna aortic valve, with a diameter of 25 mm and manufactured by

Edwards Lifesciences in California, was used. This valve is composed of bovine pericardium and an Elgiloy frame. The mechanical properties of bovine pericardium, including its stress-strain curve, have mainly been obtained by carrying out experimental techniques such as uniaxial and biaxial tensile tests [31–33]. Nonetheless, the planar tests are not sufficient to completely capture the mechanical behavior of soft tissue that occurs outside of the plane, and to obtain accurate properties that are perpendicular to a surface, it is essential to use different ways of deforming materials under normal physiological strain rates [34]. Furthermore, the mechanical characteristics of materials evaluated during pre-clinical trials can vary significantly from those of the materials utilized in implanted bioprosthetic valves, owing to notable variations within and between specimens [35]. Thus, using accurately optimized material parameters that precisely represent the mechanical response of the leaflets specific to the valve is crucial in computational simulations. Our objective was to create a framework for characterizing materials using both experimental and numerical methods to determine the mechanical properties of soft tissue employed in BHVs. As a result, we evaluated the three-dimensional isotropic mechanical properties of the leaflets found in commercially available bioprosthetic heart valves, CE PERIMOUNT Magna aortic valve.

1.5.3. FSI Analysis

FSI approaches are typically categorized in two types:

1. Monolithic or direct approach: In this approach the equations that govern the structure and fluid are solved simultaneously in a one matrix. The Monolithic approach is always stable since the influence of fluid and the structure on each other are taking into account directly. The Monolithic approach has been used in Adina [36,37].

2. Partitioned or staggered approach: In this approach the fluid and structure equations are solved separately while exchanging data at the FSI interfaces. The coupling algorithm in this approach depends on the interaction between the structure and the fluid. Partitioned coupling algorithm is separated into weak and strong algorithms. In weak coupled

algorithm or explicit, we exchange data one time in each time step, while in strong coupled algorithm or implicit there are multiple subiteration in each time step between structure and the fluid until we have the convergence with desired error. Stability is one of the most important issues in the partitioned approach. Instability usually depends on not only mass density of the fluid against mass density of the structure, but also the domain geometry [38]. The stability of the implicit approach is usually higher than the explicit approach and it's not highly dependent to the time step, while in implicit approach there is a limitation for the time step. On the other hand, explicit coupling is so expensive and time consuming [38]. In the explicit Fluid structure interaction (FSI) simulation of heart valves coupling, we usually use under-relaxation for the stabilization [37].

Also, the techniques used to simulate dynamic boundaries can be broadly grouped into two categories. Boundary-conforming methods, in which it is necessary to incorporate the grid velocity into the formulation, like ALE formulation [39]. The process of mesh movement can be computationally expensive, particularly for intricate 3D geometries. In contrast, non-boundary-conforming methods utilize a static grid that remains fixed in place within the fluid domain, without adapting to changes in the boundary's shape or position. Instead, to enforce the appropriate boundary conditions at a moving boundary, forcing terms can be introduced into the governing equations of fluid motion. These terms are added either explicitly or implicitly. [40,41]. Peskin developed a pioneering non-boundary-conforming technique, called the classical immersed boundary method [40,42,43], which was originally created for simulating blood flow through the heart and heart valves. In a study by Girifith [44], a second-order accurate adaptation of the immersed boundary method was introduced that is specifically designed to simulate cardiac blood-muscle-valve mechanics. The effectiveness of this approach is evaluated, and it is shown to be an extension of a uniform grid method. Timing results show reduced computational resources with adaptive mesh refinement. Borazjani [36] conducted a FSI simulation of BHV through an finite element solver, which incorporates a Fung-type nonlinear constitutive law that is anisotropic, to model BHV tissue. A sharp-interface immersed boundary method is also used to simulate the flow of fluid through the BHV, while considering physiological

conditions. It’s reported that the flow through the BHV differs significantly from that of the MHV.

In a numerical study conducted by Espino et al. [45], the feasibility of developing a simultaneous fluid-structure interaction (FSI) simulation for the mitral valve using an Arbitrary Lagrangian-Eulerian (ALE) approach with genuine multi-physics coupling was investigated. The model includes a simplified geometry with a heart chamber but has limitations as it cannot directly simulate chordae tendineae, which are crucial for mitral valve function. Stress distributions may be affected by chordae tendineae modeling, with 3D models being more sensitive to their inclusion. Nevertheless, the model's outputs are in agreement with empirical findings, such as a maximum radial strain of 12.6% at a pressure equivalent to 120 mmHg (16 kPa), which align with previous studies. Several investigations have described a computational framework for fluid-structure interaction (FSI) that integrates a variational immersed-boundary method with the conventional Arbitrary Lagrangian-Eulerian (ALE) technique [46,47].

1.6. Impact Of Using Commercial Software Packages for Cardiovascular Simulations

The use of commercial software packages for modeling and simulations, particularly in the context of heart valves, can have several impacts compared to in-house codes.

1. One-on-one support guaranteed by commercial source: commercial software is developed and maintained by a company that you have an established relationship with. They will guarantee that your software works properly. In contrast, many open-source software programs lack proper manuals or documentation, thus implementing and maintaining an open-source system may require a more experienced team compared to a commercial system. Generally, open-source software receives minimal support, and there is no guarantee that customizations made by one party will work with other customizations. This responsibility falls on you to test the complete solution [48].

2. File sharing: It is simpler to share files since it is probable that other users are utilizing the same software [49].
3. Diverse methods: Usually, several solvers are available, which can be chosen according to the type of problem [50].
4. User-friendly interface and simplicity: As vendors rely on customers to purchase their software, it is crucial to create software that is user-friendly. Moreover, since there are numerous open-source software alternatives, developers must offer a good user experience. As a result, the software is easy to use [51,52].

Overall, the impact of using commercial software packages versus in-house codes in heart valve modeling and simulations can vary depending on factors such as ease of use, robustness, reliability, updates, support, cost, and customization requirements. Researchers and practitioners need to carefully evaluate the specific needs and goals of their study and consider these factors when choosing between commercial software packages and in-house codes for their modeling and simulation needs.

CHAPTER TWO: BOVINE PERICARDIUM DENSITY AND IT'S IMPLICATION on BHVs COMPUTATIONAL MODELING

2.1. Introduction

Bioprosthetic heart valves (BHVs) are a non-invasive promising treatment option for people suffering from heart valve disease. BHVs do not demand long-term anticoagulant therapy while they have better hemodynamics as compared to mechanical heart valves[53,54]. Bovine pericardium (BP) is one of the common materials in manufacturing BHVs which includes a high amount of layered proteins (collagen and elastin)[33,53–55]. In BHV implants fabrication, picked BP patches are cut into leaflet shapes to apply onto sewing rings to form BHVs. It has been shown that valve performance is highly dependent on leaflet material properties. Considering and analyzing these characteristics is of interest to many researchers. In 1998, Hiester et al. [35] examined the optimal sections of BP for use in BHV by investigating 20 BP sacs. An optimal BP site for BHV needs to have low-fiber preferred direction variation across the site and negligible amounts of fat. Hiester et al. used small-angle-light scattering (SALS) to report the fiber architecture and preferred direction distribution. They found some regions in all BP sacs that meet criteria. In addition, they indicated that each BP sac has considerable variation in the location and fiber orientation of the optimal sites. Structural valve degeneration is the primary cause of failure in bioprosthetic valves.

There have been two primary procedures aimed at preventing SVD in pericardial valves. The first is the development of anti-calcification treatments that can slow or prevent leaflet calcification. The second area of focus involves modifying the method of leaflet suspension in order to reduce mechanical stress. Almost all of the currently available BHVs utilize glutaraldehyde (GA) fixation in their fabrication. GA fixation results in cross-linking of collagen and antigen (chemical stabilization) reduction, and also reduces

immunogenicity when implanted. GA fixation at high-pressure distorts crimp geometry and matrix fragmentation—causing stiffening and kinks in valve leaflets. Thus, fixation is usually done under physiological pressure to minimize these problems[56,57]. After fixation with glutaraldehyde, free aldehyde groups and phospholipids remain in the tissue, which can promote calcium deposition and subsequent calcification. If untreated, this process can lead to rapid and severe deterioration of the valve [11]. In 2011, Gilberto et al. [56] worked on other chemical approaches to prepare an acellular bovine pericardium matrix for BHVs production. They utilized an alkaline extraction in calcium salts for cell removal. Gilberto et al. observed that while they had cell removal after 12 hours, collagen fibril structure and stability to collagenase increased after 24 hours of the process. Their results revealed a process for manufacturing tissue valves and tissue reconstruction. In 2017, Tam et al.[55] investigated the effect of replacing Glutaraldehyde with an irreversible, carbodiimide-based crosslinking chemistry (TRI) to increase valve performance regarding calcification and tissue degeneration. They observed that TRI curb calcification like other solutions, while providing more robust tissue through stabilizing more of the tissue ECM. The tissue is more compliant and resists permanent deformation and degeneration. Likewise, in 2018, Meuris et al.[58] introduced a novel treatment for reducing the mineralization of BPHV to increase tissue durability by using an aldehyde-free solution for tissue storage (free-treated precordium). They compared mechanical and biomechanical characteristics of the treated valve with samples from commercially available biological values (Trifecta and Perimount Magna). They observed that the novel treated pericardium's mechanical strength and biomechanical properties are related to mentioned commercial valves. They revealed that mitral implants of novel-treated valves in sheep had great hemodynamic performance at five months without any calcification. They concluded their treatment Improve the anticalcification properties of bioprosthetic valves and can potentially enhance their long-term durability.

The widely recognized Perimount bovine pericardial valves manufactured by Edwards Lifesciences originally used the XenoLogiX tissue treatment, involving a phospholipid removal from the leaflets through a two-steps process [59]. It was shown by

Cunanan et al.[59] that the aforementioned treatment proved effective in removing above 90% of the phospholipids from the leaflets; notably, these leaflets serve as calcification binding sites. The anti-calcification procedures have been growing and improving during the past three decades at Edwards. In order to fix, sterilize, and decrease pericardial leaflet antigenicity, buffered glutaraldehyde and FET (formaldehyde-tween 80 solution) are employed by the TFX (Thermafix) method [60]. The Perimount Magna Ease tissue valve has used the same process. A novel treatment has been offered by Edwards recently, based upon perpetual blocking of all interactions with calcium by capping the free-aldehydes. Subsequently, glycerolisation occurs on the tissue with the purpose of substituting any remaining molecules of water with glycerol. A 72% decrease in calcium was achieved through application of this tissue (a.k.a., the "Resilia" tissue) in a Perimount valve, relative to a valve in a juvenile sheep model treated via TFX [61]. In the period of 2013–16, 689 patients received Perimount Magna Ease valve implants through the COMMENCE trial, which were reformed to entail the Resilia tissue [62]. Data over the subsequent four years demonstrated desirable hemodynamic performance and safety (with mean gradients of 11.0 ± 5.6 mmHg, effective orifice areas of 1.5 ± 0.5 cm^2, and no cases of SVD [63]).

On the other hand, other studies investigated the mechanical properties of different sections of bovine pericardium. In 1998, Hiester et al.[35,64] examined 20 BP sacs to locate optimal BP sections for use in BHV. An optimal BP site for BHV needs to have low-fiber preferred direction variation across the site and negligible amounts of fat. They used small-angle-light scattering (SALS) to report fiber architecture and preferred direction distribution. They found some regions in all BP sacs that meet the criteria. They also noted that each BP sac has considerable variation in location and fiber orientation in the optimal sites.

In vitro studies play a significant role in describing the mechanical properties of soft tissues as well as computational modeling validation. Finite element analysis (FEA) has been widely used to study prosthetic and natural heart valves, reducing the costly and lengthy process required for in vivo and in vitro analysis [33]. Finite element (FE) simulation is a powerful tool in the analysis of heart valve durability. In numerical

simulations of BHVs, some challenges include leaflet contact and nonlinear anisotropic leaflet mechanical properties. Experimental tests exist to validate results [63,65]. Utilization of actual leaflet material properties—such as mechanical properties, damping coefficient, and density—is essential for accurate BHV FE simulations. Bioprosthetic leaflet mechanical properties are shown to be mechanically anisotropic [28]. Different numerical simulations of heart valves showed that the anisotropic Fung model is a reliable model in BHVs simulations that can accurately predict valve deformation during opening and closing of the valve. Abassi et al.[66] utilized inverse FE methods to determine anisotropic material constants of bovine pericardial leaflets of a surgical bioprosthetic heart valve. Like other BHV mechanical properties (Isotropic and anisotropic mechanical models), BHV density has a considerable impact on leaflet stress and strain distribution. Previous computational studies assumed BP density to be close to the density of water or blood (1000–1100 kg/m3). However, BP leaflets undergo multiple treatments as described earlier. In 2013, Borazjani [67] studied a Fluid-Structure Interaction (FSI) simulation of bio-prosthetic heart valves by using immersed boundary Navier-Stokes (NS) equations for the fluid domain and a large deformation FE method for the structure. In this study, three shells with a density of 1060 kg/m^3 and a thickness of 1 mm were considered for the leaflets. They reported a considerable difference between the blood flow field passing through the tissue valve and mechanical valve during the heartbeat cycle. Small-scale vortical structures were observed in the mechanical heart valve before the peak of systole, but not in the bio-prosthetic heart valves. The results of incomplete transcatheter aortic valve (TAV) expansion on the leaflets stress and strain distribution was considered using FEA [31]. In this study, 1100 kg/m^3 was considered the leaflet's density. It was observed that different sizes of incomplete expansion of TAV stent can make localized high-stress regions within the commissure and belly of TAV leaflets. Another study considered the effect of geometry on leaflet stresses in Bicuspid aortic valves (BAV) using FEA [68]. Material properties obtained from porcine aortic valve leaflets were employed for the simulation. A density of 1100 kg/m^3 and thickness of 0.386 mm was set in Abaqus FEA software. Significant changes in leaflet strain and stress were observed with variations in

the geometry of simulated BAV. They concluded that calcific aortic stenosis, which frequently exists in patients with BAV, may result from geometrical variations.

The goal of the present work is to measure the density of bovine pericardial patch and analyze the impact of density on BHV leaflet stress and strain distribution. To do so, we conducted an FE analysis of surgical valves by using the anisotropic Fung model and measured density. Finally, we optimized the material coefficients of the Fung model with the new density. To the best of our knowledge, this is the first study to measure the density of commercially available bovine heart valves and compare leaflet deformation and stress with different densities.

2.2. Method

2.2.1. Experimental Testing

The density of Edwards bovine pericardial patch (Model 4700, Edwards Life Sciences, CA) used in BHVs was directly measured in the present study. Accordingly, eight specimens were cut from two bovine pericardium patches (four from each patch). A Fusion M2 40 (Epilog Laser, CO) laser cutter was employed to excise square-shaped specimens (10×10 mm), and patches were stored in a saline container. A tissue thickness value of 0.5 mm ± 0.25 mm is reported on the Edwards Lifesciences website [69]. A dial caliper (Fowler 52-008-712-0, Canton, MA) was used to measure all edges of the specimens. In addition, pictures were taken from the specimens on a piece of Teflon and were processed using Photoshop to determine sample length and thickness more accurately. Specimen dimensions were measured with ±0.01 mm accuracy.

To measure leaflet density as blood passes through, we put the leaflets in a solution with the human blood density. Accordingly, water was mixed with glycerol 99% to produce a solution with blood density (1.056 g/ml) at normal human body temperature (37℃). The volume ratio was 9.0 ml for glycerol and 31.0 ml for the water, as previously reported by Glycerine Producers' Association [70].

We considered two procedures for measuring the weight of the samples. In the first one, sample weight was measured inside of the prepared solution. Consequently, specimens were placed in the solution with blood density to measure the weight after removing the container droplets. In the second procedure, sample weight was measured by directly placing samples on the Analytical Balance (A&D GR-202, Gurgaon, Haryana). The Analytical Balance used in this study had an accuracy of 10^{-4} g.

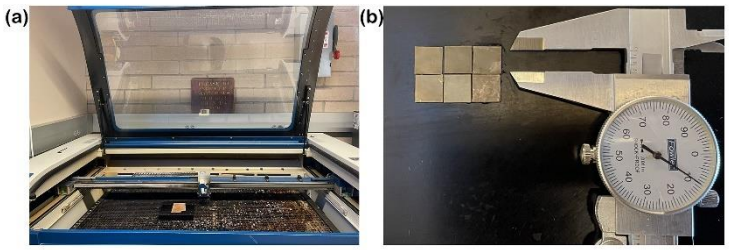

Figure 2- 1- a) Fusion M2 40 laser cutter and samples b) Samples thickness measuring using dial caliper.

2.2.2. Computational Modeling

An FE analysis was conducted on the effect of density deviation on the deformation and stress distribution of PERIMOUNT Magna aortic heart valve (Edwards Life Sciences, CA)−a well-known and commercially available surgical valve. For this purpose, we conducted a dynamic analysis on the 25 mm PERIMOUNT Magna Bioprosthesis with five different densities−1,000, 1,100, 1,200, 1,300 and 1,410 kg/m3−based on our finding in the first part of the study. A NextEngine 3D Laser Scanner was also employed to obtain the geometry of the surgical valve leaflets [55]. Meshing was done using Hypermesh. The valve leaflets and the wire frame stent were discretized via approximately 7,700 quad elements (S4) and 400 beam elements, respectively (Fig. 2). Mesh independency was done through three different element numbers.

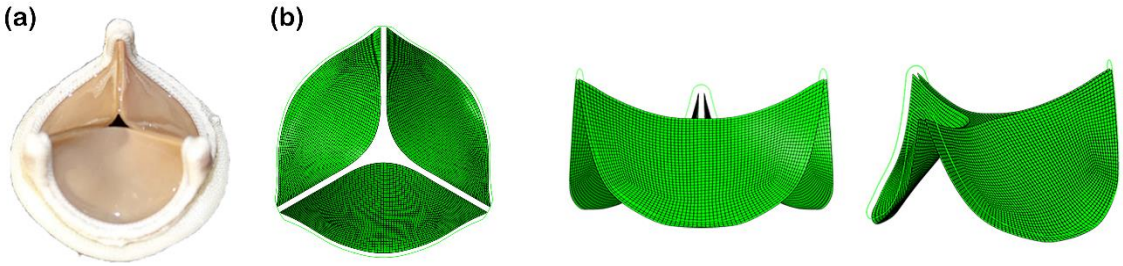

Figure 2- 2- (Left) 25-mm Perimount magna surgical bioprosthetic aortic valve and the FE model showing the leaflets geometric configurations attached to the stent.

Abaqus/Explicit was used to carry out the FE analysis. Material orientation was given to the leaflet's elements utilizing a MATLAB code [71]. A thickness of 0.56 mm was taken into account in the simulations. According to the literature, viscous damping effect of the fluid around the BHV should be considered in the FE analysis via Rayleigh damping [25], which helps achieve a smooth non-oscillatory convergence of the finite element method. Therefore, the Rayleigh damping coefficient was considered as α=10642 1/s in this study [71]. A non-linear anisotropic Fung-type elastic constitutive model was employed for the leaflets:

$$w = \frac{c}{2}(e^{Q} - 1), \qquad Q = E : (\text{Þ}E) \tag{2-1}$$

where E is the Green–Lagrange strain tensor, and Þ is a non-dimensional symmetric tensor entailing 21 independent coefficients of the Fung model.

$$\begin{bmatrix} b_{1111} & b_{1122} & b_{1133} & b_{1123} & b_{1113} & b_{1112} \\ & b_{2222} & b_{2233} & b_{2223} & b_{2213} & b_{2212} \\ & & b_{3333} & b_{3323} & b_{3313} & b_{3312} \\ & & & b_{2323} & b_{1323} & b_{1223} \\ & Symmetric & & & b_{1313} & b_{1213} \\ & & & & & b_{1212} \end{bmatrix}$$

Pressure waveform obtained from a previous study using in vitro analysis (Figure 2-3) was used as the simulation physiological loading condition [66].

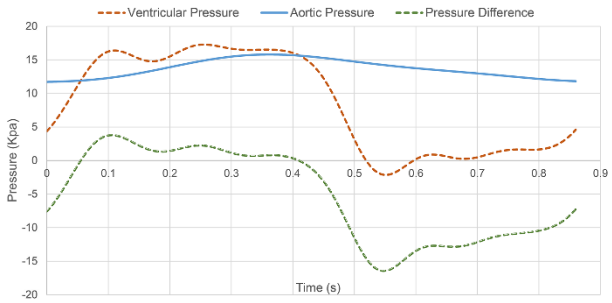

Figure 2- 3- Pressure wave frame.

A material optimization was carried out for the leaflets, based on the deformation experimental results of previews study by Mostafa et al. [71] The experimental hemodynamic results obtained from setting up a 23 mm paramount Magna valve in a pulse duplicator system. A high-speed camera was employed to capture the valves' leaflet motion at 960 FPS. The center of each leaflet was tracked, and the distance between the center of the leaflet and the center of the valve was calculated through the opening and closing of the valve. The PSO method from Isight and Abaqus was used in this study as the optimization procedure. Accordingly, the distance between the center of the leaflet obtained from the simulation with the corresponding measurements obtained from the pulse duplicator system (experimental measurements). The optimization was forced to stop when the objective function's change reduced to less than the tolerance value of 10^{-5}.

2.3. Results

2.3.1. Density Measurement

Square samples of constant size were cut from the bovine pericardium patch and stored in the saline solution. Table1 shows the length and thickness of each sample from patches 1 and 2. The results of mass measurements are shown in Table 1, as well. As visible, the weight of each sample measured using method 2 is higher than method 1 due to solution absorption in the samples.

Table 2- 1- Dimensions and volume of specimens; mass of specimens and density of bovine precordium patch

	Case Number	Thickness (mm)	X (mm)	Y (mm)	Volume (mm^3)	Weight measured directly(g)	Weight in B Solution(g)	Density: measured directly (g/cm^3)	Density: Samples in the solution (g/cm^3)
Patch 1	1	0.55	9.80	9.81	52.4619	0.0681	0.0735	1.23	1.40
	2	0.57	9.78	9.85	54.9098	0.0622	0.0783	1.13	1.43
	3	0.56	9.78	9.85	53.9464	0.0611	0.0672	1.13	1.26
	4	0.63	9.67	9.67	58.9106	0.0759	0.0815	1.29	1.38
	mean	0.58	9.76	9.79	55.0572	0.0667	0.0751	1.20	1.37
	SD	0.04	0.06	0.08	2.7592	0.0069	0.0062	0.068	0.064
Patch 2	1	0.485	9.68	9.81	46.05599	0.0622	0.0674	1.35	1.46
	2	0.49	9.70	9.8	46.5794	0.0654	0.0699	1.40	1.50
	3	0.51	9.55	9.78	46.6995	0.0660	0.0642	1.41	1.37
	4	0.50	9.51	9.65	45.8375	0.0620	0.0681	1.35	1.49
	mean	0.49	9.6075	9.76	46.2931	0.0639	0.0674	1.38	1.46
	SD	0.01	0.0977	0.0744	0.4126	0.0020	0.0023	0.027	0.056

Additionally, the density of each sample and the average for each different patch is shown in Table 1. The standard deviation (SD) for the density for all specimens is less than 0.07, indicating that the values are close to the mean of the set. Finally, by measuring the mean of bovine precordium patch density, in the two different processes, the values 1,300 kg/ m^3 and 1,410 kg/m^3 are reported for the first and second measurement process respectively. As discussed in the method, the second method in measuring the density is more reliable and 1,410 kg/m^3 was used as our reference density in our PERIMOUNT Magna Ease valve simulations and material optimization. As mentioned in the introduction, in previous simulations and analyses, 1000 kg/ m3 and 1100 kg/m^3 [67,68,72,73] were used for both bovine and porcine precordium density. Thus, we compared the stress and strain on the leaflets - the most important surgical valve longevity analysis with different densities (1,000, 1,100, 1,200, 1,300, 1,410 kg/m^3) in both systole and diastole.

2.3.2. Leaflet Stress and Strain Distributions

Fig. 2.4a and 2.4b show the maximum value in plane principal stress (MPPS) distributions of the 25 mm premium Magna surgical valve with different density at the acceleration and deceleration. Since dynamic motion exists in the opening and closing of

the valve, results were analyzed during acceleration and deceleration. As is visible, the leaflet stress distribution was dependent on the density of the leaflets. Table 2 includes MPPS and the percentage change in the MPPS on the leaflets with 1410 kg/m^3 density in comparison with four other densities in acceleration and deceleration. The magnitudes of the MPPS in acceleration are much larger than the corresponding magnitudes in the deceleration. In the acceleration, high-stress regions were detected in the fixed edges between middle of fixed edge and commissure, and the maximum principal stress reached to 1.91 MPa for the valve with the 1410 kg/m3 density. As expected, the amount of higher density shows lower stress during the systole. In addition, higher density reduces the acceleration of the leaflets, achieving lower deformation and stress. As presented in Figure 2.4a, lower density (incorrect density) induced localized high stress and strain regions on the fixed edges of the leaflets in the acceleration. The presence of incorrect density resulted in two local stress concentration spots on the fixed edge site and increased the max in plane stress to 2.47 MPa (more than 30% difference). However, high-stress regions were observed mainly near the commissures during deceleration, and the maximum stress reached 0.713 MPa. Decrease in density from 1410 kg/m^3 to 1000 kg/m^3 resulted in decreased magnitudes of the maximum principal stress in the deceleration.

As shown in Figure 2.5, the maximum amount of deformation occurred in the middle of moving edge, the amount of displacement reaches 6.55 mm during acceleration. By considering 1410 kg/m^3 as a reference value for density, the difference of assuming 1,000, 1,100, 1,200 and 1,300 kg/m^3 as density will be remarkable (more than 13%). We have the highest magnitude in case 1 (density = 1,000kg/m^3). The difference not only happens in acceleration but can be seen in deceleration. The max displacement results for different density cases in deceleration are shown in Figure 2.6. As seen in the figure, the contrary acceleration of the highest displacement is case 5. The computed maximum displacement magnitude and U2 of node one (middle of moving edge) results were then compared for different densities in Table 3. The largest change in the maximum displacement based on

the density variations in the BHVs models was 13 %, and 11% in acceleration and deceleration respectively.

Also, these results show that the maximum in-plane stress and displacement occur in case 1 (density=1,000 kg/m^3) compared to other cases in acceleration, while it occurs in case 5 (density =1,410 kg/m^3) in deceleration.

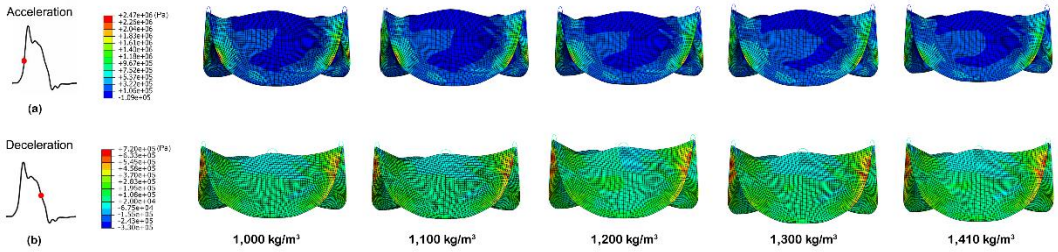

Figure 2- 4-Max in plane principal stress of 25 mm premium Magna surgical valve in the acceleration and deceleration with different density ranging from 1000 kg/m^3 to 1410 kg/m^3.

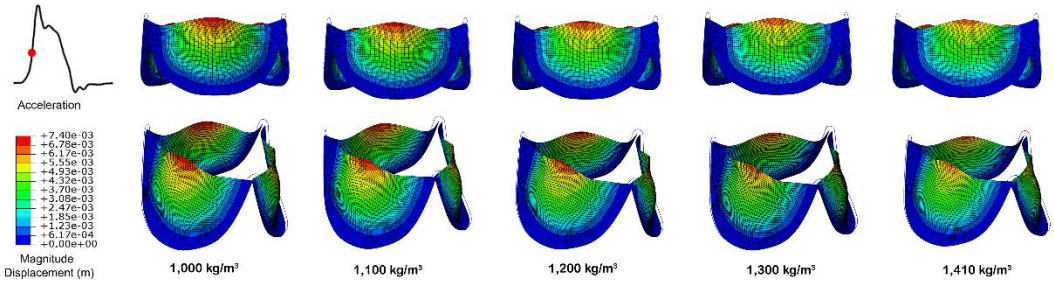

Figure 2- 5-Displacement magnitude of 25 mm premium Magna surgical valve in the acceleration with different density ranging from 1000 kg/m^3 to 1410 kg/m^3.

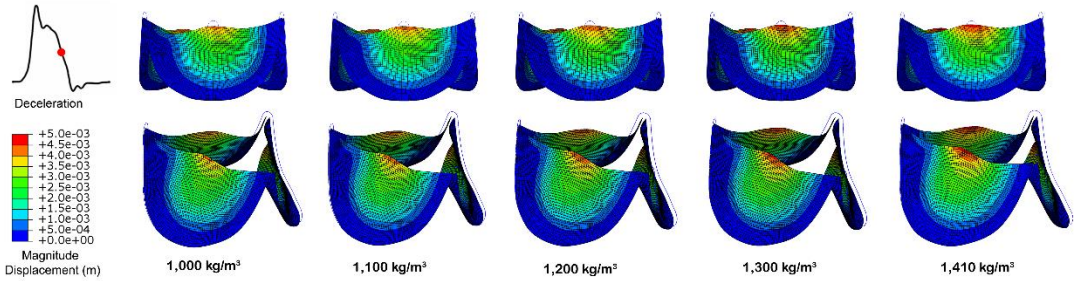

Figure 2- 6- Displacement magnitude of 25 mm premium Magna surgical valve in the deceleration with different density ranging from 1000 kg/m^3 to 1410 kg/m^3.

Table 2- 2- Max in plane stress detected in acceleration and deceleration with different density (ranging from 1000 kg/m^3 to 1410 kg/m^3).

Acceleration	Max in plane stress	Difference (%)	Deceleration	Max in plane stress	Difference (%)
Density=1000	2.47E+06	30.7	Density=1000	6.69E+05	6.17
Density=1100	2.32E+06	22.8	Density=1100	6.81E+05	4.48
Density=1200	2.06E+06	9	Density=1200	6.92E+05	2.95
Density=1300	1.91E+06	1.06	Density=1300	7.02E+05	1.55
Density=1410	1.89E+06	0	Density=1410	7.13E+05	0

Table 2- 3- Magnitude and Node 1 displacement in the acceleration and deceleration with different density ranging from 1000 kg/m^3 to 1410 kg/m^3.

Acceleration	U mag. (mm)	Difference (%)	U2 of node 1	Difference (%)	Deceleration U mag. (mm)	Difference (%)	U2 of node 1	Difference (%)
Density=1000	7.4	13	6.72	14.67	4.27	11.05	3.61	13.22
Density=1100	7.21	10	6.54	11.6	4.42	7.92	3.76	9.61
Density=1200	7	6.87	6.33	8.02	4.56	5	3.9	6.25
Density=1300	6.8	3.82	6.11	4.27	4.68	2.5	4.03	3.125
Density=1410	6.55	0	5.86	0	4.8	0	4.16	0

2.3.3. Material Optimization

The 3D mechanical properties of the Magna premium valve were optimized based on the displacement from the experimental results obtained from the pulse duplicator system. In-plane displacement of the middle point of the middle edge in the FE simulation in Abaqus was matched with the experimental results. Initial and optimized material coefficients are shown in the following. The displacement results were obtained after two optimizations (initial optimization and optimization) with different initial parameters showed a proper match with the experimental results [71]. A perfect agreement in the opening and closing and the slope can be seen in Figure 2.7.

Initial material components of Fong model reported in the literature for the 25 mm PERIMOUNT Magna [71]:

$$\begin{bmatrix} 63.42 & 31.84 & 51.29 & 17.37 & 49.02 & 39.39 \\ & 63.74 & 46.75 & 68.38 & 63.09 & 19.22 \\ & & 62.82 & 38.51 & 60.17 & 55.50 \\ & & & 14.30 & 15.47 & 28.04 \\ & Symmetric & & & 47.30 & 13.69 \\ & & & & & 67.53 \end{bmatrix}$$

Optimized material components of Fong model found for the 25 mm PERIMOUNT Magna with 1410 kg/m^3 density:

$$\begin{bmatrix} 65 & 30.519 & 46.338 & 15.81 & 46.29 & 38.554 \\ & 60 & 44.38 & 71 & 51 & 16.6 \\ & & 77 & 41.32 & 69.89 & 43 \\ & & & 12 & 11.245 & 31.95 \\ & Symmetric & & & 46.05 & 9 \\ & & & & & 67 \end{bmatrix}$$

Table 2- 4- Material parameter for the 3D anisotropic Fung model

	C	α
Paramount Magna (Initial coefficients)	90720	10642
Paramount Magna (Optimized coefficients)	59000	2642

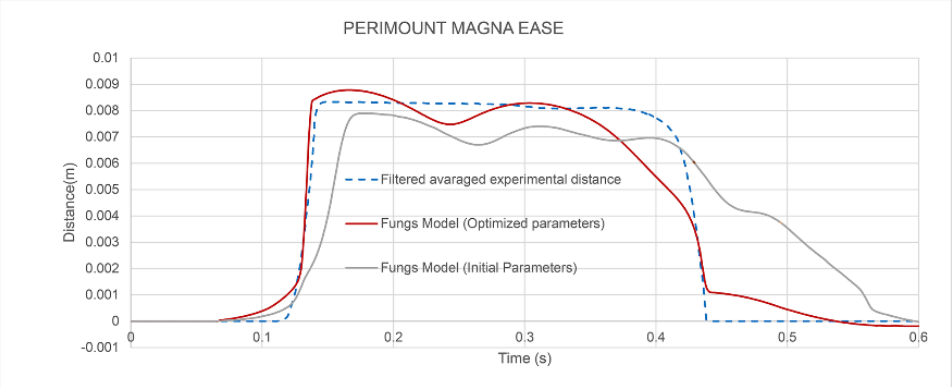

Figure 2- 7- Middle point displacement of the leaflet for the three valves; comparing optimized FE simulations with the experimental data.

2.4. Discussion

This study improves understanding of the structural performance of surgical heart valves. Stress distribution and deformation of the BHV leaflets depend on the magnitude of density; by considering 1410 kg⁄m^3 as the reference value for density, the difference of taking the value of 1000 kg⁄m^3 into account as the density value would be remarkable. Relevant differences in stress distribution have a strict correlation with different kinematics of the leaflets. In computational models, it is essential to consider an accurate value for the density of BHV leaflets.

Computational modeling and FE analysis in particular are significantly strong tools for evaluating and optimizing the durability of BHVs through displacement and stress analysis. To obtain the mechanical behaviors of bioprosthetic aortic valve leaflets, accurate properties of tissues are essential, helping us design and manufacture novel prosthetic valves.

Calcification of the prosthesis is the main issue faced by bovine pericardial valves; these problems can result in stenosis in the valve leaflet and may ultimately cause failure. Glutaraldehyde (GA) fixation is commonly used in the fabrication of existing bioprosthetic valves [57]. Notably, pericardium anisotropy is considerably decreased by the GA fixation process [74]. There are newer approaches in the form of novel multistep procedures aimed at anticalcification. New procedures are developed to reduce rate of calcification, including valve fixation using nonglutaraldehyde crosslinking agents; calcification prevention through prostheses treatment via trivalent metal ions or 2-alpha- amino-oleic acid; or the application of surfactants or ethanol to eliminate materials with calcification potentials [75].

Utilizing experimentally derived material properties in finite element (FE) models and simulate valve deformations under physiological conditions can be used to improve the design and long-term durability of bioprosthetic heart valves (BHV). In this study, we overlooked variability with regards to the three leaflet material properties in simulations of three bioprostheses aimed at lowering the computational time. Furthermore, to imitate the surrounding fluid, viscous damping was applied in FE simulations. Simulating the interaction between fluid and structure could offer a simulation with a higher level of precision which we will consider in future studies. Also, adding more samples could increase the accuracy of our experiment. Thus, more robust findings could be achieved from experiments involving more patches.

CHAPTER THREE: FSI SIMULATION AND EXPERIMENTAL VALIDATION OF BIOPROSTHETIC HEART VALVES

1.5. Introduction

Bioprosthetic heart valves (BHVs) are a non-invasive promising treatment option for people suffering from heart valve disease. BHVs do not demand long-term anticoagulant therapy while they have better hemodynamics as compared to mechanical heart valves their durability and hydrodynamic is still an issue. For BHVs development, extensive and costly pre-clinical and clinical testing is required, which limits the opportunity to refine the design of BHVs and explore new ideas. In the past decade, computational modeling has become more crucial in the design and development of BHVs. Computational modeling is one of the strongest tools for evaluating and optimizing durability and hydrodynamic performance of BHVs through analyzing deformation, stress distribution, velocity, vorticity, shear stress and other factors. FSI simulations have increasingly played a significant role in analyzing the fluid mechanics of heart valves in recent years. FSI simulations enable the analysis of the interaction between blood, surrounding biological tissues, and the valve itself. Coupled Fluid-Structure Interaction (FSI) simulations involve the interaction between the structure and fluid domains, which results in outcomes from both domains. Fluid-structure interaction (FSI) simulations are used to analyze the fluid mechanics of heart valves, and the choice of using either an arbitrary Lagrangian-Eulerian (ALE) or Eulerian formulation (Immersed Boundary Method) in describing the discretization of the fluid domain was discussed by Bavo et al [44]. The study was the first to compare the performance of arbitrary Lagrangian-Eulerian (ALE) and immersed boundary (IB) methods for solving the fluid-structure interaction (FSI) problem of an aortic valve, and to report on the advantages and disadvantages of both methods specifically for aortic valve case. In this study, the authors set up 2D and 3D aortic valve models using both the ALE and IB method and

compared their performances. According to the study, the differences between the 2D cases were not significant. However, they observed a considerable time delay in the motion of the leaflets in the 3D modeling using the IB method for FSI simulations while the IB method did have a significant advantage in terms of computational cost. In the present study, we have developed a 3D FSI computational model representing a surgical bioprosthesis (25-mm PERIMOUNT Magna Ease) inside a pulse duplicator system (BDC Labs). The simulation results were validated against experimental data obtained by particle image velocimetry (PIV) measurements.

3.2. Method

3.2.1. Experimental Pulse Duplicator

To evaluate the hemodynamics of a 25mm Carpentier-Edwards Perimount bioprosthetic aortic valve, a pulse duplicator system designed by BDC Labs in Wheat Ridge, CO was utilized. The system, which operates at room temperature, ensures that the testing environment is precisely controlled and consistent, making it an effective tool for assessing valvular hemodynamics. The pulse duplicator system was configured to meet both ISO-5840 standards and FDA guidelines for testing heart valves. Specifically, the testing conditions were set to a heart rate of 70 beats/min, with mean atrial and aortic pressures of 10 and 100 mmHg, respectively, and a cardiac output of 5 L/min. To simulate blood, a recirculating solution consisting of 37% glycerin in normal saline (by volume) was used. The solution was carefully formulated to match the density (1094 kg/m^3) and viscosity (0.0035 Ns/m^2) of blood at human body temperature. To measure pressure in the aorta and left ventricle during testing, strain gauge pressure transducers were utilized. These transducers were embedded within the pulse duplicator system, positioned 35mm upstream and 105mm downstream of the bioprosthetic aortic valve. The mean pressure gradient of the 25-mm CE PERIMOUNT Magna bioprosthesis was found to be 8.6 ± 0.07 mm Hg. To determine the outlet boundary condition, pressure in the aorta was measured, while flow rate was measured as the inlet boundary condition. The motion of the valve leaflets was recorded using a high-speed camera (SONY DSC-RX10M3) at 960 frames per second, and the resulting images were digitized using MATLAB. The center of each leaflet

was tracked throughout the cardiac cycle, and its distance from the center of the valve was calculated.

A conventional two-dimensional PIV system was employed to acquire planar velocity measurements downstream of the bioprosthetic valves. The PIV system was illuminated by a dual oscillator Nd:YAG laser (Litron Lasers Nano S 15 Hz), with the lasers being synchronized using a Laser Pulse. PIV data was collected alongside leaflet deformation data and used to validate the measurements obtained. Please note that for more details you can refer to Barakat et al. [79].

3.2.2. Numerical Analysis

To evaluate the hydrodynamic and durability performance of the 25 mm Paramount Magna aortic heart valve, 2-way fluid-structure interaction (FSI) simulations were conducted. The simulations involved four steps. Firstly, the geometry was created, and finite element analyses were performed using the transient structural module of Ansys with different constitutive law formulations to identify appropriate constitutive laws and accurate material parameters based on experimental leaflet deformation. In the second step, the structural analysis of the valve was carried out using the transient structural module of the Ansys Workbench. This involved simulating the mechanical behavior of the valve's leaflets, including their deformation and stresses, in response to the forces coming from the fluid solver of the FSI simulation. In the third step, the Fluent module of the Ansys Workbench was used to set up the fluid section of the simulation. This involved modeling the flow of blood through the valve and simulating the hydrodynamic behavior of the valve, such as flow velocity, pressure drop, and turbulence. Finally, in the fourth step, the Ansys system coupling module out of the Ansys Workbench was utilized to perform the 2-way coupling between the fluid domain and structure. This allowed for the interaction between the mechanical and fluid behavior of the valve to be fully captured, accounting for the impact of the fluid flow on the valve's deformation and vice versa. The 2-way FSI simulation aimed to provide a comprehensive evaluation of the valve's performance, including its durability, hemodynamic performance, and overall functionality under

realistic physiological conditions. In the following, each step of the simulation process is explained in detail.

3.2.2.1. Leaflets geometry and 3D Finite element Analysis

As one of the recent most reliable surgical heart valves, the Carpentier-Edwards PERIMOUNT Magna bioprosthesis valve has been proposed in this study. To reconstruct the geometry of the leaflets, a 3D laser scanner (NextEngine, Santa Monica, CA) was used. The resulting data was then processed using Geomagic Design X to create a 3D model of the leaflets. After creating the splines, the final geometry was generated in SolidWorks by using the lofted surface feature to create the leaflet, based on the splines. The average thickness of the leaflets, which was measured using digital calipers, was determined to be 0.54 mm and was used in the subsequent analyses. Numerical modeling and especially FE has proven to be a powerful tool in increasing our understanding of the physiological response of prosthetic heart valve leaflets under physiological boundary conditions [9-14]. However, the development of accurate simulation of the mechanical behavior of these leaflets relies heavily on the appropriate formulation of constitutive laws and the precise identification of their material parameters [15]. In addition, a better understanding of the fundamental ventricular mechanics requires a realistic depiction of the myocardium's three-dimensional geometry and microstructure, including boundary conditions, as well as the use of constitutive equations that accurately characterize the material properties of the myocardium [16].

3.2.2.2. Optimization

In this study a global optimization approach was used to determine the 3D mechanical properties of the leaflets. Different hyperelastic isotropic models available in Ansys, Mooney Rivlin, Yeoh 3rd order, Ogden 1st order, Ogden 2nd order, polynomial 2nd order, and polynomial 3rd order, were used as different models to find the best model and define the mechanical properties of the leaflets. Abaqus curve fitting was utilized for the initial estimates of the material coefficients. Stress-strain curves obtained from equibiaxial

stretch conditions were utilized for this purpose [31]. These initial estimates were used as a starting point of the optimization.

I used Gateway Isight for optimizing the mechanical properties coefficients. The raw hemodynamic data, the leaflets tip deformation, obtained from the pulse duplicator system, was utilized for the optimization [71].

The material coefficients were determined by optimizing the error norm of displacement field between measurements of leaflet tip deformation and Finite Element (FE) simulations. This was achieved using the particle swarm optimization (PSO) method, using Isight (Simulia, Providence, RI).

In the optimization process, the objective function was determined as the average sum of squared differences between the displacement values obtained from experimental results and simulation results. Convergence was achieved after approximately 200 iterations. The optimized material coefficients were then used to generate displacement contour plots, which were compared with the experimental displacement contours obtained from the camera. The optimization process was programmed to stop when the change in the objective function fell below the preset tolerance level of 10^5.

3.2.2.3. 3D Fully Coupled FSI Simulation

In this part, the different parts of the FSI modeling are presented, and it includes both the fluid and structural domains and system coupling. Ansys Workbench 2021 was used to predict the computational domain due to its capability to analyze the computational domain and exchange data between flow and structural solvers. For solving the structural part of the simulation ANSYS Transient structural was used and for fluid dynamics ANSYS Fluent was used. System coupling 2021 R2 was used for exchanging data at the fluid-structure interface between ANSYS Fluent and ANSYS Transient structural in our simulations. The structure and fluid equations and their interaction were discussed in the following.

Solid mechanics solver (Transient structural):

In section 3.2.2.1, we provided an explanation of the process used to derive the geometry of the leaflets. HyperMesh (Altair Engineering, Inc., Troy, MI) FE pre-processor was employed to discretize the geometry using a mapped mesh with 18538 hexahedral elements [0.12mm mesh] (Figure 3-1).

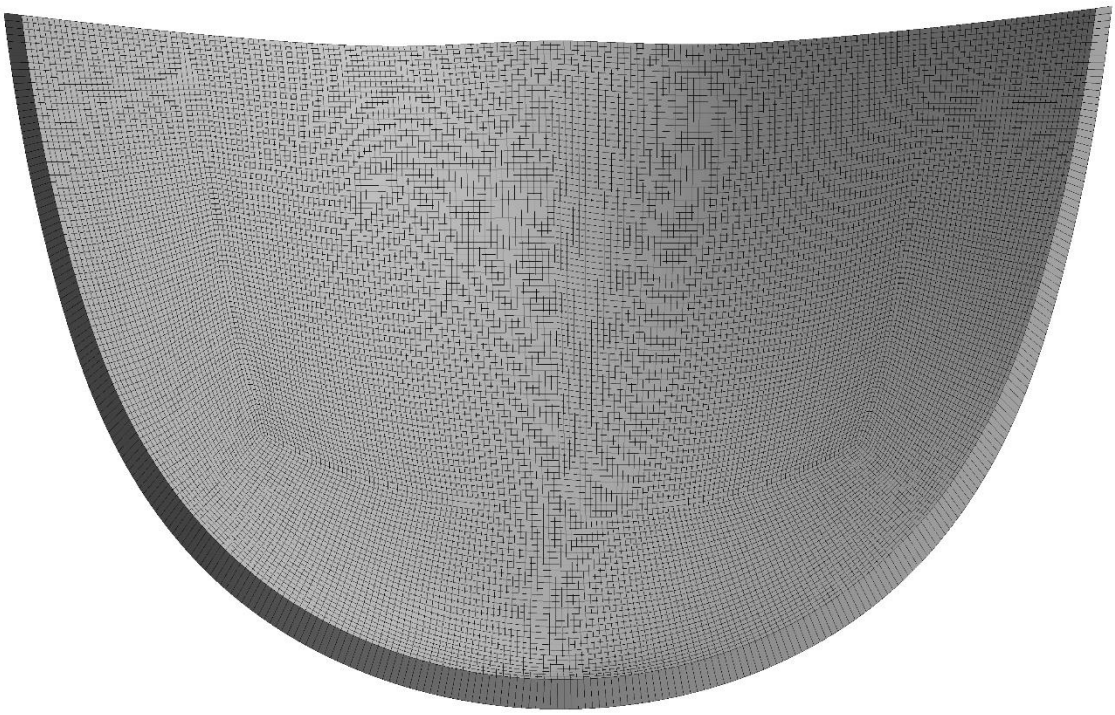

Figure 3- 1- Structure (leaflet) computational mesh

The mesh was then imported to Ansys Transient structural. Bioprosthetic leaflets were considered to be hyperplastic isotropic materials. Yeoh 3rd order strain energy function was developed as a framework to model the mechanical behavior of the leaflets. The strain energy potential is:

$$W = \sum_{i=1}^{3} C_i \, (I_1 - 3)^i \qquad (3\text{-}1)$$

where C_i are the mechanical constants of the material found using optimization and I_1 is the first deviatoric invariant of the deviatoric right green deformation tensor. The density of the leaflets was 1410 kg/m^3 considered based on our recent experimental study.

3.2.2.3.2. Flow Solver (Fluent)

The considered 25-mm surgical Carpentier-Edwards PERIMOUNT Magna aortic valve is placed over a geometry model of the custom build pulse duplicator.

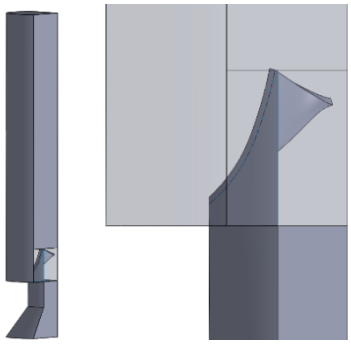

Figure 3- 2- (a) Computational model; (b) Magnification of leaflet area

Fluid (blood flow inside the pulse duplicator) meshing was done using pointwise. The fluid domain was discretized via approximately $1.2*10^6$ tetrahedral element.

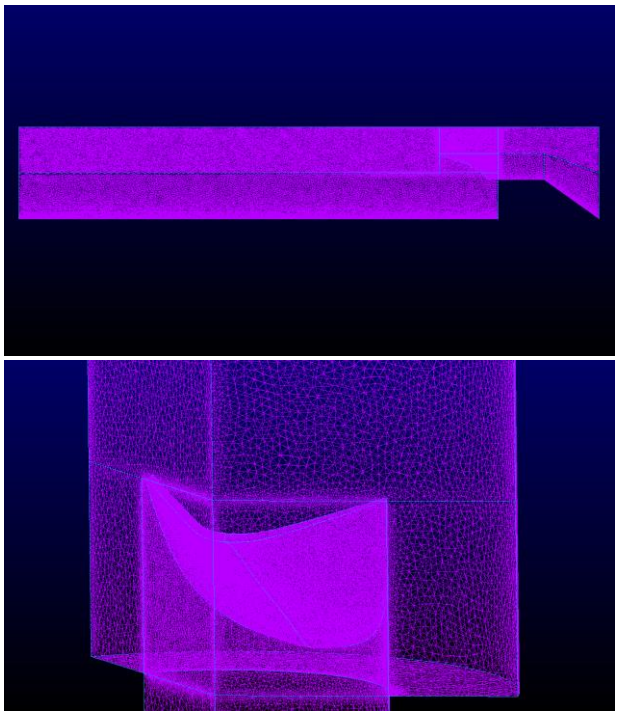

Figure 3- 3- Fluid computational mesh

Mesh independency for both the structure and fluid mesh was done through three different element numbers. To ensure accurate data transfer between the fluid and structure domains in FSI simulations, it is necessary to have a fine enough mesh grid that can capture the phenomena occurring in the interfaces. Using identical mesh grids for fluid and solid domains around the FSI interfaces is also recommended. As a result, the mesh grid near the leaflets needs to be finer, and generating almost identical mesh grid in FSI interfaces is attempted.

The blood passing through was specified as a homogeneous, Newtonian incompressible fluid with a density of ρ = 1060 kg/m3 and a viscosity of η = 0.0035 Pa. Additionally, the methodology for solving the governing equations is described along with the applied boundary conditions. For discretizing the computational system, ALE formulations were used. The governing equations for this case are Navier-Stokes (NS) equations. The equations are written in tensor notation, in which i and j =1, 2,3.

$$\frac{\partial U_i}{\partial t} + \frac{\partial (U_j - \widehat{U}_j) U_i}{\partial t} - B_i - \frac{1}{\rho}\frac{\partial P}{\partial x_i} + \frac{1}{\rho}\frac{\partial \tau_{ij}}{\partial x_i} \tag{3-2}$$

Where ρ, $\bar{U}$, U, P, B, μ are the density, interface boundary velocity, instantaneous velocity vector, pressure, body force, and dynamic viscosity of the fluid respectively, besides the fluid density has been assumed to be 1050 kg/m^3.

The turbulence parameters were studied by considering the Unsteady Reynolds-Averaged Navier-Stokes (URANS) equations:

$$\rho\frac{\partial u_i}{\partial t} + \rho\frac{\partial (u_j - \hat{u}_j)}{\partial x_j} = \rho B_i - \frac{\partial P}{\partial x_i} + \frac{\partial}{\partial x_j}(\mu\frac{\partial u_i}{\partial x_j} - \overline{\acute{u_\iota}\,\acute{u_j}}) \tag{3-3}$$

u and $\hat{u}$ in equation 2 are the mean velocity and the velocity fluctuation in a turbulent field.

Hence the total stress based on the URANUS formation can be written as :

$$\overline{\tau_{\iota J}} = \mu\left(\frac{\partial u_i}{\partial x_j} + \frac{\partial u_j}{\partial x_i}\right) - \rho\overline{\acute{u_\iota}\acute{u_J}} \tag{3-4}$$

In this relation, the second-order tensor $-\rho u_i' u_j'$ is the Reynolds stress tensor, which is unknown, can be calculated using the Boussinesq approximation or the turbulent viscosity hypothesis, so it can be correlated to the mean flow field. This results in the total stress taking the following form:

$$\overline{\tau_{ij}} = \mu\left(\frac{\partial u_i}{\partial x_j} + \frac{\partial u_j}{\partial x_i}\right) + \frac{2}{3}\rho k \delta_{ij} - \mu_t\left(\frac{\partial u_i}{\partial x_j} + \frac{\partial u_j}{\partial x_i}\right) \quad (3\text{-}5)$$

where the eddy viscosity for turbulent, μ_t can be determined. To calculate this parameter, the Realizable k-w model is utilized as the flow through the aortic valve undergoes transition to turbulent flow. Transport equations for turbulent Kinetic energy, k, and its dissipation rate, w through this model are solved. Because it is able to predict complex flows with important strain rates like recirculation and strong pressure gradient the transient simulation of the hemodynamic performance of BMHVs can be conducted too.

The viscosity associated with eddies or turbulence is characterized as:

$$\mu_t = \rho C_\mu \frac{K^2}{\varepsilon} \quad (3\text{-}6)$$

where variable Cμ is depends on the tensors of strain and vorticity rate. Now, by utilizing these relations, Kinetic energy and its dissipation rate can be obtained by solving the transport equations. For modelling flow through small gaps there is an option in Ansys called gap model. I used the gap model to simulate the blockage of flow when a gap is closed in the diastole. A gap region is made up of a pair of face zones, so that when one moves within a specified proximity threshold distance of the other, the fluid cells within the threshold of the zones are marked, and then the flow is blocked at the boundary faces of the marked region so that the marked cells no longer participate in the solution (for what is called a flow-blocking type region). The 0.28 mm was used for the gap model threshold since we defined 0.28mm gap in our model (SOLIDWORKS). The model was added in Figure 3-4.

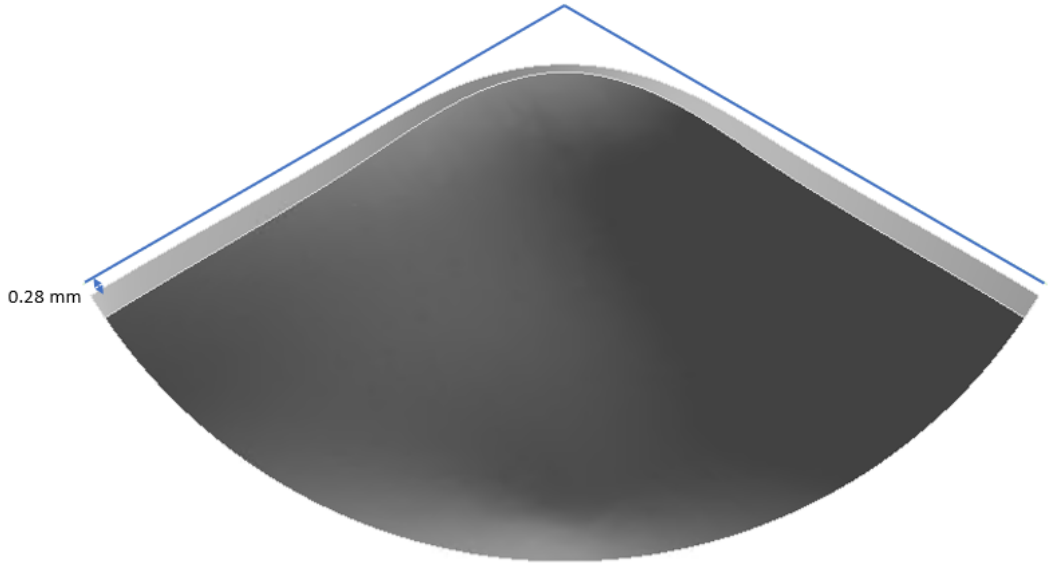

Figure 3- 4- Gap in the fluid domain

In the Dynamic mesh, we enabled Smoothing and Remeshing. For Smoothing, I've used Spring/Laplace/boundary method. For remeshing I've used local cell in the remeshing methods. For the parameters, I've used mesh scale info for the parameters. In the dynamic mesh zones, I've selected Fluid solid interfaces (leaflet faces) as System coupling. In the solution methods, I've used simple as the Scheme, and Standard for the pressure spatial discretization. Also, the first order implicit was used as the transient formulation.

The flow rate and pressure waveform obtained from a previous study using in vitro analysis (Figure 3-5) was used as the simulation physiological loading conditions [66]. The physiological flow rate represented by the blue line has been set as the inlet boundary condition, and the red line was set as pressure outlet in the pulse duplicator.

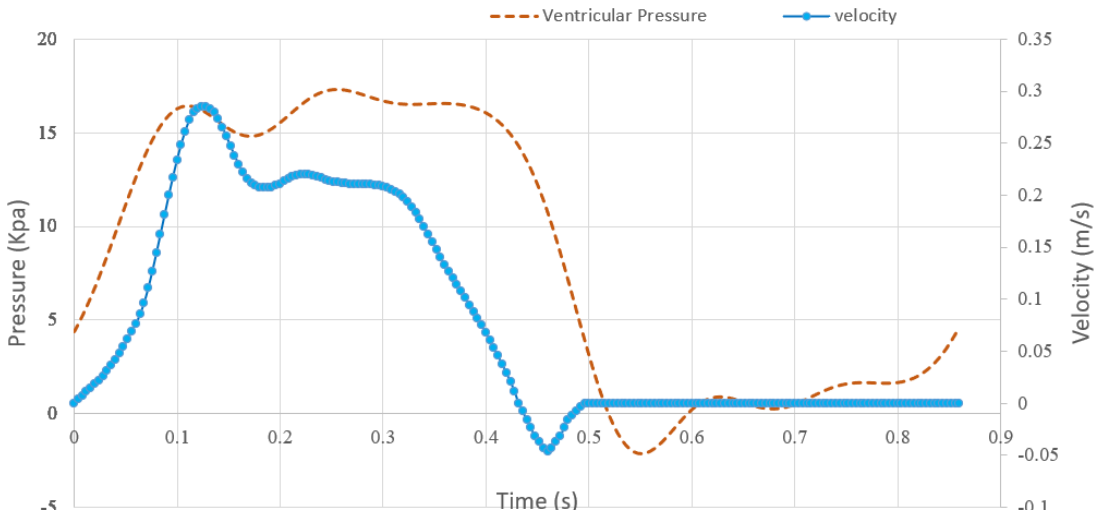

Figure 3- 5- Velocity and Pressure wave frame.

3.2.2.3.3. Fluid Structure Interaction (System Coupling)

Dynamic condition (or traction equilibrium) and Kinematic condition (or displacement compatibility) are the important conditions that are applied to the coupling interfaces. The equations are mentioned as the following:

$$d_f = d_s \tag{3-7}$$

$$n.t_f = n.t_s \tag{3-8}$$

where d_s and d_f respectively are solid and fluid displacement, n is the unit normal vector, t_s, and t_f are the solid and fluid stresses, respectively. We have performed the coupled analysis outside of the Ansys Workbench using System Coupling 2021 R2 module. In this way, we have access to more options and consequently greater control over files and setups. Quasi-Newton has been chosen to have more stability in the global stabilization and the minimum number of iteration and the maximum was chosen to be 1 and 10 respectively in the solution control.

Our simulations employed the segregated approach to solve the fluid and structure systems separately while exchanging data at the fluid-structure interface. FSI interfaces were assigned to leaflet surfaces in this study. In the solution control of the system coupling, the end time is after 2 cycles, 1.92 s, the initial time step size is 0.001s while it's from 0.002 and 0.0001 based on the circulation phase. Given that both the fluid and solid

models are interdependent and exchange data with each other, we utilized two-way coupled FSI using the ALE method in our simulations. As boundary displacement, the leaflet deformation communicated to the flow from transient structural. Thus, Fluent has been used to solve the governing equations in the updated flow field. Next, the forces acting on the solid domain were transferred from Fluent to Ansys transient structural. Next, the equations governing the behavior of the valve leaflet are solved. The system coupling and data transition in each time step are illustrated in Figure 3-6.

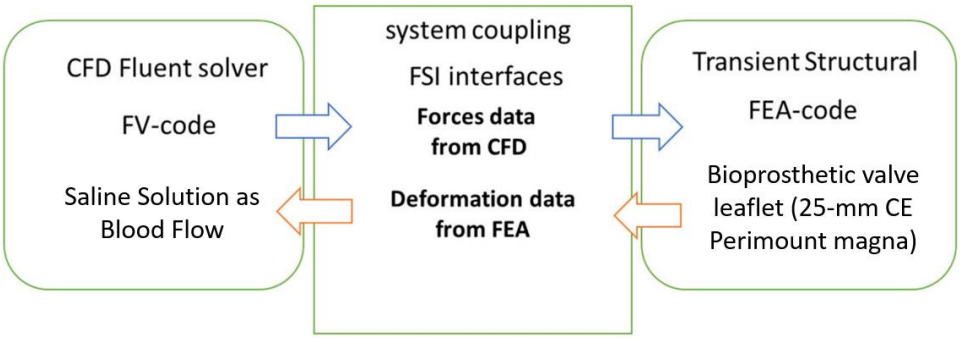

Figure 3- 6- Flow chart of data exchanging in each FSI iteration.

The process of iterative exchange of data between Ansys Fluent and Ansys mechanical in the CFD-FEM solver will continue until a converged solution is reached in each FSI iteration. It is worth mentioning that the analyses consumed around 330 h on 48 processors with 3.5 GHz frequency and 40 Gb of Ram.

3.3. Results

Coupled Fluid-Structure Interaction (FSI) simulations involve the interaction between the structure and fluid domains, which results in outcomes from both domains. In other words, the simulation generates results from both the structural and fluid domains that are coupled and affect each other.

3.3.1. Material Optimization

Optimal material coefficient of Yeoh 3rd order model was found after 200 iterations reported in table 3.1. The displacement results with optimized material showed a proper match with the experimental results [71]. A perfect agreement in the opening and closing and the slope can be seen in Figure 3-7.

Table 3- 1-. Optimized material coefficients of the Yeoh 3rd order model.

Parameter	C1	C2	C3	Incompressibility parameter
value	848025	-12252084	388346628	5.2e-6

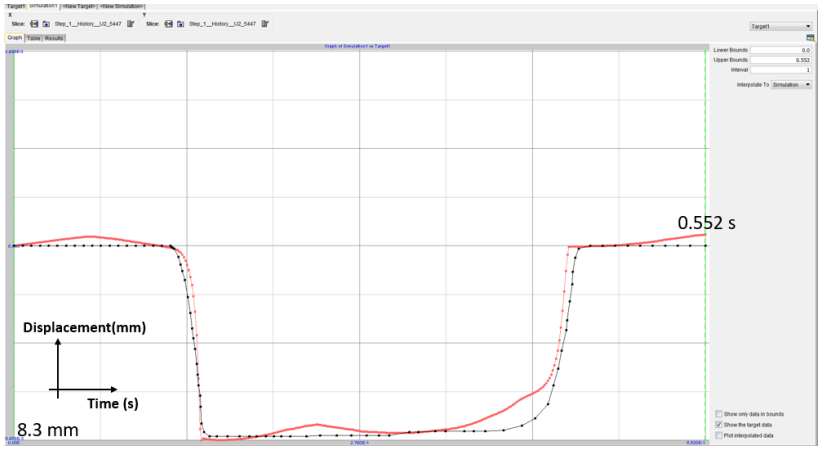

Figure 3- 7-Middle point displacement of the leaflet; comparing optimized FE simulations with the experimental data.

3.3.2. Fluid and Structure Results

To assess the hemodynamic performance of bioprosthetic heart valves, it is crucial to analyze various factors such as velocity profile, flow pattern, shear stress, and wall shear stress. Accurate evaluation of these factors is vital in ensuring the effectiveness and reliability of bioprosthetic heart valves. Also, validating the developed framework using experimental analysis was done in the following.

Velocity Contour and Shear stress

The flow contour at different time points is shown in Figure 3-8. The results are presented in 6 parallel horizontal cross sections during five distinct phases of a cardiac cycle: acceleration, peak systole, deceleration, early-diastole, and mid-diastole. The results come from the second cycle of the simulation. As it can be seen, during the acceleration and pick systole, the velocity along the centerline of the bioprosthetic exhibited high axial flow, 1.86 m/s and 2.06 m/s respectively, but there was a substantial decrease in velocity from the central jet to the surrounding area. During the deceleration phase, the velocity of the jet at the core decreased to 1.5 m/s. The velocity magnitudes were observed to decrease considerably after valve closure during both the early- and mid-diastole phases.

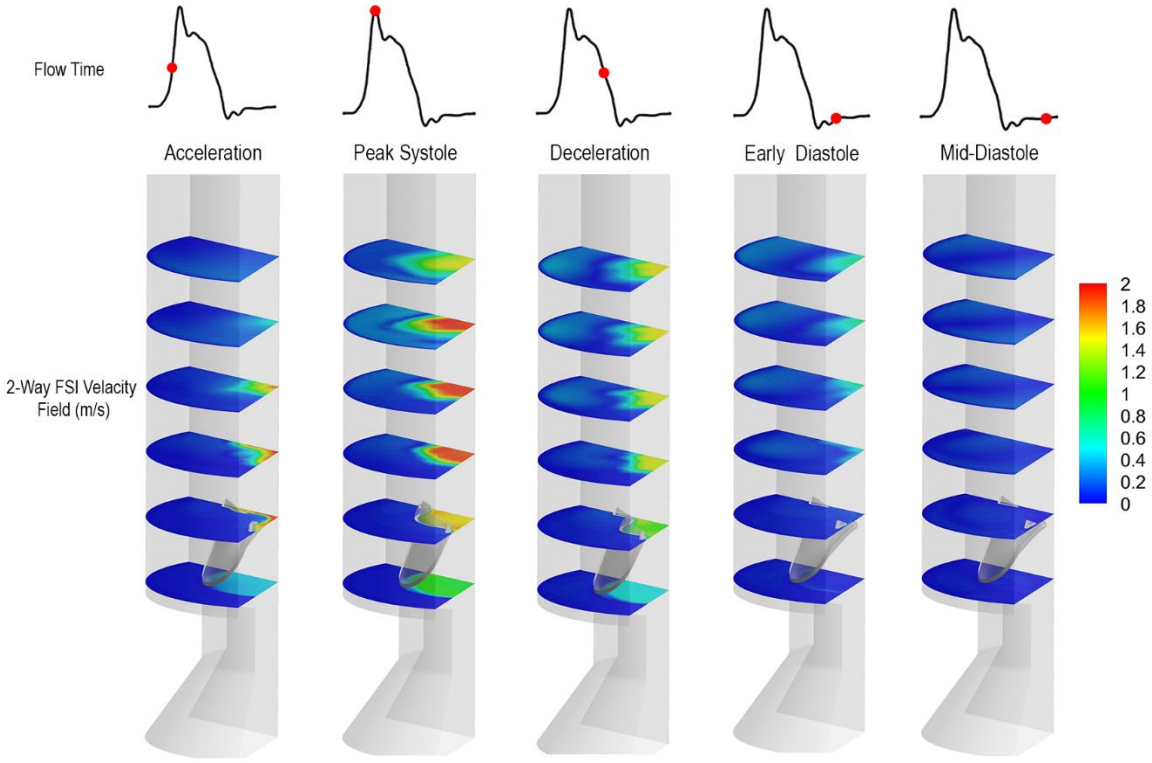

Figure 3- 8-Velocity magnitude contours at different horizontal cross-sections.

Figure 3-9 illustrates a comparison between the velocity contour obtained from a two-way Fluid-Structure Interaction (FSI) simulation and experimental analysis (PIV) of the 25-mm Carpentier-Edwards PERIMOUNT Magna bioprosthesis. As can be seen there is a great agreement between PIV and 2-way FSI. At the peak of flow, the maximum jet velocity in

FSI and PIV were 2.06 m/s and 2.1 m/s, and the jet diameter was approximately 15.2 mm and 1.45 mm In PIV and FSI respectively. The plane at which the flow parameters is the mid-plane cutting through the bioprosthetic valve. Good agreement between the experiment and the simulation results was observed. Viscous shear stress fields in both PIV and FSI were shown in the right side of Figure 3-8. At the peak systole, the jet boundary layer experienced a maximum viscous shear stress of 4 N/m2 along a significant portion, However, the magnitude of the shear stress was notably lower during the deceleration phase than at the peak flow in both PIV and FSI results.

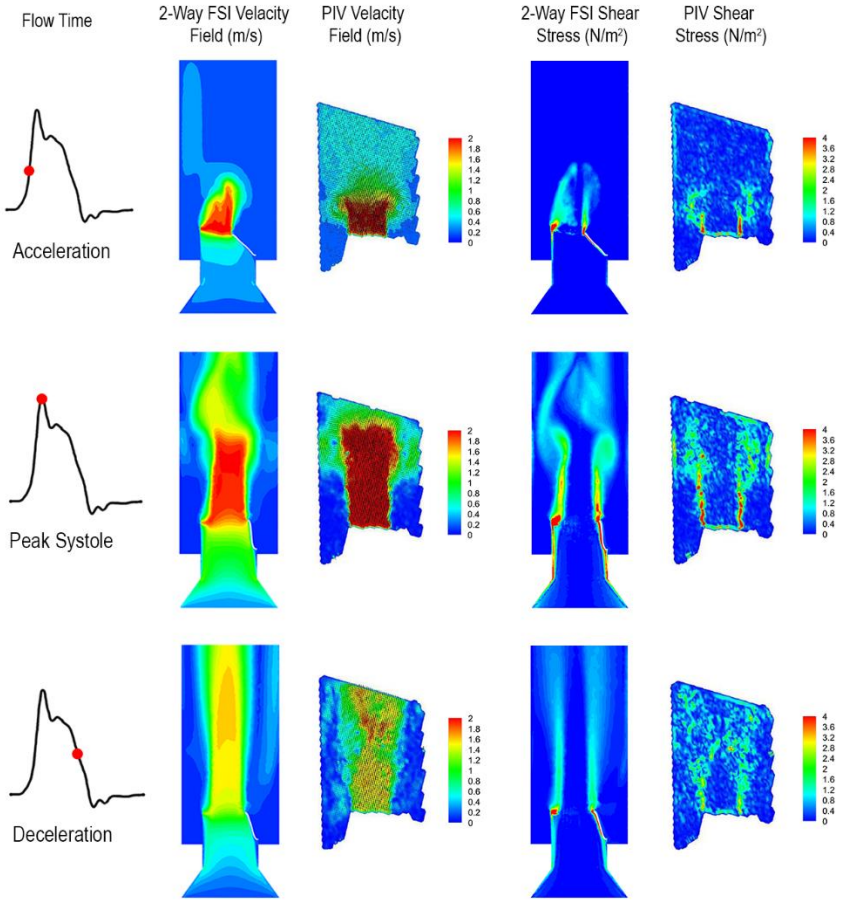

Figure 3-9- Comparison of instantaneous velocity and viscous shear stress fields of a 25-mm carpentier-Edwards Perimount magna bioprosthesis during various phases of the cardiac cycle, determined by experimental and numerical analysis.

Wall Shear Stress

As one of the thrombosis formation factors, the wall shear stress on the leaflet was investigated. Figure 3-10 shows the wall shear stress on the aortic and ventricular sides of the leaflet. The result indicates that the shear stresses on the ventricular side of the leaflet were generally higher than on the aortic side. The maximum shear stress was 106 Pa.

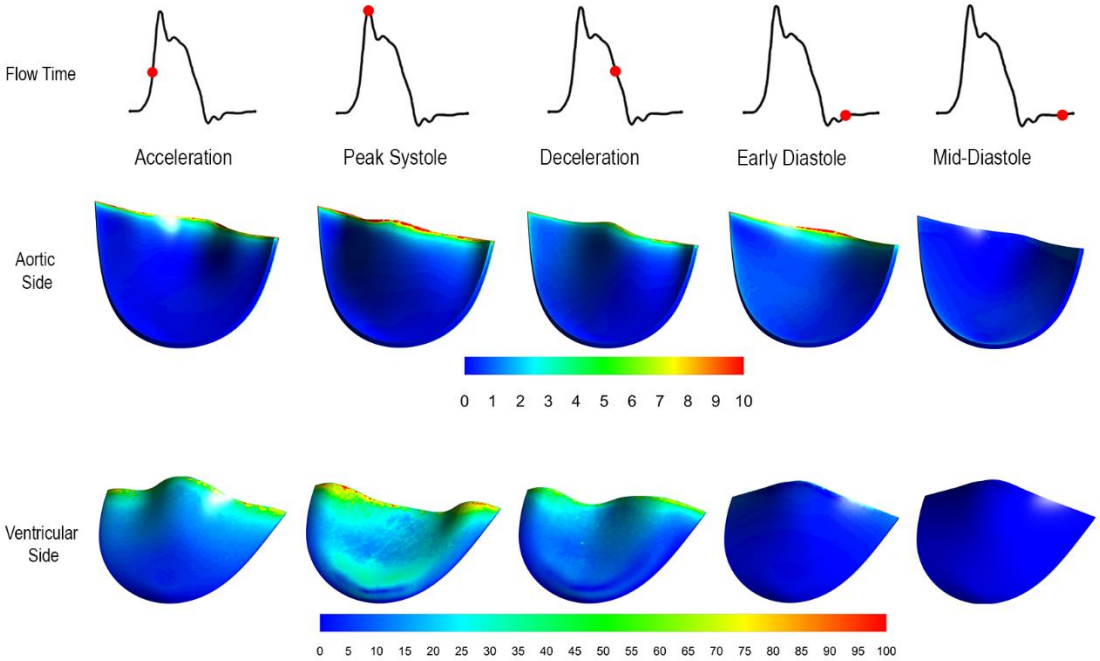

Figure 3- 10- Wall shear stress on the leaflet, top: aortic side; bottom: ventricular side.

Stress and strain on the leaflets

FSI simulations can provide the results for both the fluid and the structure. The stress and strain distribution of the 25mm Premount Magna valve during the peak systole and mid diastole are displayed in Figure 3-11. The figure demonstrates that the distribution of stress and strain in the valve leaflet were changed considerably during a cardiac cycle. In peak systole, areas of high stress are primarily concentrated along the boundary edge, with a maximum principal stress of 0.357 MPa when the valve is fully open. In mid diastole, however, high-stress regions are primarily observed at the commissures, with a maximum stress of 0.028 MPa. Similarly, the distribution of the maximum principal strain

follows a similar pattern during valve opening and closing. The maximum strain value at the boundary edge reached 0.06 when the valve was fully open (peak systole), and it reached approximately 0.01 at the commissures during mid diastole.

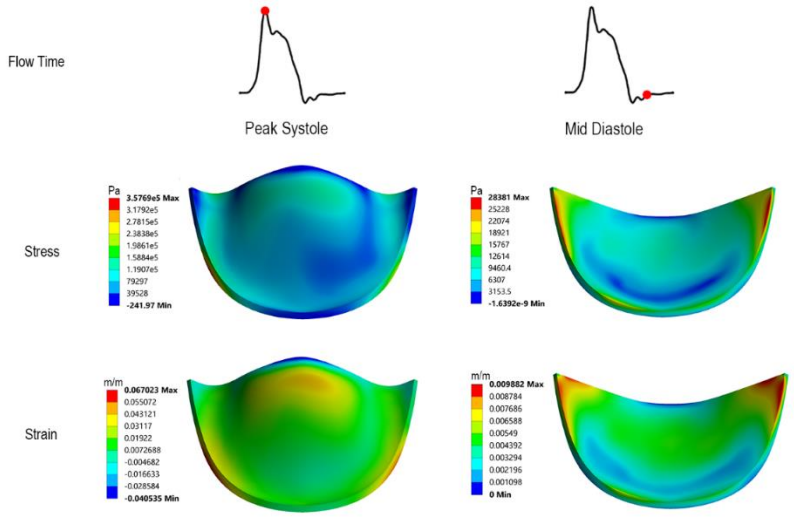

Figure 3-11- Leaflet stress and strain distribution in Peak Systole and Mid Diastole.

3.4. Discussion

The study created Fluid-Structure Interaction (FSI) models of BHVs within an In-vitro test system (pulse-duplicator). The leaflet models were designed with isotropic descriptions of the leaflet biomechanics derived from optimization techniques. Furthermore, experimental pressure and flow data collected from the pulse-duplicator systems were employed to establish accurate boundary models for the detailed FSI models. Fluid dynamics is a crucial factor in causing problems related to clotting and hemolytic issues in prosthetic heart valves [80,81]. These issues have been linked to areas of high shear stress in the blood flow, where hemolysis and platelet activation can occur [82]. The force of shear stress experienced by blood cells is primarily caused by viscous shear stress rather than Reynolds shear stress when there is turbulence [7]. The duration and magnitude of shear stress are both important factors in the activation of blood cells. It has been established that the threshold level of shear stress that causes no damage to red blood cells, irrespective of exposure time, is 150 N/m^2 [83]. The recorded shear stress caused by viscosity downstream of the valve was well below the established threshold level for damage to red blood cells found in previous studies.

To summarize, this study focused on modeling BHVs within an experimental pulse-duplicator platform that is employed in diverse settings to evaluate their functionality. Experimental in vitro testing has played a significant role in verifying and optimizing the design of medical devices. However, in recent years, the significance of computational modeling has increased significantly for designing and verifying prosthetic heart valves. This trend has been largely driven by regulatory bodies such as the U.S. Food and Drug Administration (FDA) and the EU Medical Device Regulatory System [84,85]. As a result, experimental in vitro testing, such as the one presented in this study, can be utilized to verify and validate computational simulations[86,87]. A combined approach that integrates experimental testing and computational modeling should be pursued to gain a better understanding of the flow-induced mechanisms that cause thrombosis in BHVs. The developed platform in this study, could be expanded and verified for its suitability in studying the efficacy of TAVR devices that exhibit decreased leaflet mobility, different levels of intra- and paravalvular leakage, and valve thrombosis [88].

CHAPTER FOUR: DISCUSSION and CONCLUSION

In summary, in the first study a rigorous experimental evaluation was carried out to obtain the accurate density of the bovine pericardium patch. The impact of different densities on SHV leaflet deformation and stress distribution was taken into account. It was found that the bovine pericardium patch density is higher than the amount used in previews simulations. SHV leaflet stress and strain distributions depended on the magnitude of density. Through dynamic simulations of a 25-mm PERIMOUNT Magna aortic valve, it was shown that the maximum principal stress was considerably greater during acceleration phase of cardiac cycle than the deceleration phase in all cases. A limitation of this study is that increasing the number of specimens from each patch and the number of patches could have yielded more robust results.

In the second study, we developed an FSI simulation of a BHV in a pulse-duplicator platform. An assessment of the fields of velocity and viscous shear stress downstream of a BHV was done using 2-way FSI simulations. The study improves our understanding of structural and hemodynamic performance of BHVs. The simulation results were validated against experimental data obtained by flow velocity measurements using PIV. We found a good agreement between them. Our validated platform is applicable for different bioprosthetic and transcatheter heart valves. The highest level of viscous shear stress occurred within the jet boundary layer at the peak of flow during systole in both FSI and PIV. However, the measured values of shear stress were lower than the threshold values reported in the literature for damage to red blood cells and activation of platelets. The probability of damage caused to red blood cells and platelet activation due to shear stress during systole is minimal.

One of the limitations of this study is that the patient's individualized structure is more intricate than that of the pulse duplicator, with calcification, wall geometry, and coronary flows potentially affecting the flow field. Additionally, it should be noted that although the URANS method was utilized in this study, the use of large eddy simulation (LES) methods is considered to be more accurate for modeling turbulent flows. Therefore, the limitation of using the URANS method can be addressed in future studies by employing the LES method for better accuracy [89]. It is important to note that the use of RCR boundary condition is one of the limitations of this study. However, it also presents an opportunity for future research to explore and address this limitation. By focusing on the RCR boundary condition in future studies, it may improve the results. Additionally, an aspect that deserves attention for future studies is the consideration of stent flexibility in FSI simulations. It definitely can make some uncertainty in our results. By incorporating the evaluation of stent flexibility, we can gain a more comprehensive understanding of its impact on both structure and fluid outcomes and implications of the study [71]. Another limitation of the study is the simplification of the model to only one-third of the complete geometry, rather than considering the entire model. This approach allows for faster results specifically pertaining to one leaflet. Also, we have used ALE for method and the primary drawback associated with the ALE (Arbitrary Lagrangian-Eulerian) approach is the continuous displacement and deformation of the mesh, which must closely follow the boundary motion. This mesh-moving process can be both time-consuming and costly, particularly when dealing with three-dimensional geometries [44]. In this study, a conventional 2D PIV system was utilized to acquire planar velocity measurements downstream of the bioprosthetic heart valve.

In general, uncertainties in PIV measurements arise from factors such as cycle to cycle variation in the flow, errors in particle tracking, background noise, and flow perturbations caused by the measurement system. These uncertainties can affect the accuracy and reliability of velocity measurements in PIV, necessitating careful consideration of experimental design, image processing techniques, and calibration procedures to minimize their impact. Although the average of data from 10 consecutive cycles in this study was

presented, a future objective is to enhance the quantification of uncertainty related to cycle-to-cycle variability in the experimental data [89]. Also, in order to validate the results of the structure side of the modeling, three-dimensional digital image correlation (DIC) technique can be used in future studies [71]. Uncertainty in Fluid-Structure Interaction (FSI) simulations arises from many factors such as modeling assumptions, numerical approximations, fluid and structure properties, boundary conditions, coupling algorithms, and parameter sensitivity and specially in our simulation the results was limited to only two cardiac cycles. These uncertainties can impact the accuracy and reliability of the simulation results [89]. To mitigate them, sensitivity analyses, validation, uncertainty quantification, and robustness analyses, and running the simulation for more cycles are important for improving the confidence and reliability of FSI predictions [89]. We have yet to conduct a systematic sensitivity analysis or uncertainty quantification of the model which can be considered for future studies. Nonetheless, despite these limitations, the findings of this study still provide valuable insights into our comprehension of the potential dangers of thrombosis. This project is a step toward the experimental verification of the conducted FSI modeling for analyzing tissue heart valves. The methodology can be used effectively for the quantitative description of the structural and hemodynamic performance of BHVs and mitigate the need to conduct expensive and time-consuming pre-clinical animal testing.

REFERENCES

[1] F. Van de Vosse, M.E.H. Van Dongen, Cardiovascular fluid mechanics—lecture notes, Fac. Appl. Physics, Fac. Mech. Eng. Eindhoven Univ. Technol. Eindhoven, Netherlands. 41 (1998).

[2] J. Fine, Applied biofluid mechanics, McGraw-Hill Education, 2017.

[3] P.A. Iaizzo, Handbook of cardiac anatomy, physiology, and devices, Springer Science & Business Media, 2010.

[4] L. Waite, J. Fine, Pulsatile flow in large arteries, Appl. Biofluid Mech. 1st Ed. New York, MY McGraw-Hill. (2007) 187–221.

[5] W.C. Ober, C.W. Garrison, A.C. Silverthorn, Human physiology: an integrated approach, Pearson/Benjamin Cummings, 2004.

[6] M. Sadipour, P. Hanafizadeh, K. Sadeghy, A. Sattari, Effect of aortic wall deformation with healthy and calcified annulus on hemodynamic performance of implanted on-X valve, Cardiovasc. Eng. Technol. 11 (2020) 141–161.

[7] L. Ge, L.P. Dasi, F. Sotiropoulos, A.P. Yoganathan, Characterization of hemodynamic forces induced by mechanical heart valves: Reynolds vs. viscous stresses, Ann. Biomed. Eng. 36 (2008) 276–297.

[8] M. Nobili, U. Morbiducci, R. Ponzini, C. Del Gaudio, A. Balducci, M. Grigioni, F.M. Montevecchi, A. Redaelli, Numerical simulation of the dynamics of a bileaflet prosthetic heart valve using a fluid–structure interaction approach, J. Biomech. 41 (2008) 2539–2550.

[9] Aortic valve, (n.d.). https://www.mayoclinic.org/diseases-conditions/aortic-valve-disease/diagnosis-treatment/drc-20355122#:~:text=Aortic valve replacement typically requires,with a biological tissue valve.

[10] R. Puri, V. Auffret, J. Rodés-Cabau, Bioprosthetic valve thrombosis, J. Am. Coll. Cardiol. 69 (2017) 2193–2211.

[11] D. Balmforth, A. Dimagli, U. Benedetto, R. Uppal, Fifty years of the pericardial valve: Long-term results in the aortic position, J. Card. Surg. 36 (2021) 2865–2875.

[12] S. Arora, J.A. Misenheimer, R. Ramaraj, Transcatheter aortic valve replacement: comprehensive review and present status, Texas Hear. Inst. J. 44 (2017) 29–38.

[13] D. Schmidt, S.P. Hoerstrup, Tissue engineered heart valves based on human cells, Swiss Med. Wkly. 137 (2007) 80S-85S.

[14] E. Filova, F. Straka, T. Mirejovský, J. Mašín, L. Bačáková, Tissue-engineered heart valves., Physiol. Res. 58 (2009) S141–S158.

[15] B. Mirani, S.P. Nejad, C.A. Simmons, Recent progress toward clinical translation of tissue-engineered heart valves, Can. J. Cardiol. 37 (2021) 1064–1077.

[16] N.M. Rajamannan, Osteocardiology: Defining the Go/No-Go Time Point for Therapy, Cardiology. 139 (2018) 175–183. https://doi.org/10.1159/000485074.

[17] R. Roudaut, K. Serri, S. Lafitte, Thrombosis of prosthetic heart valves: diagnosis and therapeutic considerations, Heart. 93 (2007) 137–142.

[18] A. Kostyunin, T. Glushkova, A. Stasev, R. Mukhamadiyarov, E. Velikanova, L. Bogdanov, A. Sinitskaya, M. Asanov, E. Ovcharenko, L. Barbarash, Early postoperative immunothrombosis of bioprosthetic mitral valve and left atrium: a case report, Int. J. Mol. Sci. 23 (2022) 6736.

[19] D.F. Keefe, F. Sotiropoulos, V. Interrante, H.B. Runesha, D. Coffey, M. Staker, C.-L. Lin, Y. Sun, I. Borazjani, T. Le, A process for design, verification, validation, and manufacture of medical devices using immersive VR environments, J. Med. Device. 4 (2010).

[20] S.F.C. Stewart, P. Hariharan, E.G. Paterson, G.W. Burgreen, V. Reddy, S.W. Day, M. Giarra, K.B. Manning, S. Deutsch, M.R. Berman, Results of FDA's first interlaboratory computational study of a nozzle with a sudden contraction and conical diffuser, Cardiovasc. Eng. Technol. 4 (2013) 374–391.

[21] R. Haj-Ali, L.P. Dasi, H.-S. Kim, J. Choi, H.W. Leo, A.P. Yoganathan, Structural simulations of prosthetic tri-leaflet aortic heart valves, J. Biomech. 41 (2008) 1510–1519.

[22] J. De Hart, G. Cacciola, P.J.G. Schreurs, G.W.M. Peters, A three-dimensional analysis of a fibre-reinforced aortic valve prosthesis, J. Biomech. 31 (1998) 629–638.

[23] E.A. Patterson, I.C. Howard, M.A. Thornton, A comparative study of linear and nonlinear simulations of the leaflets in a bioprosthetic heart valve during the cardiac cycle, J. Med. Eng. Technol. 20 (1996) 95–108.

[24] K.H. Lim, J.H. Yeo, C.M. Duran, Three-dimensional asymmetrical modeling of the mitral valve: a finite element study with dynamic boundaries., J. Heart Valve Dis. 14 (2005) 386–392.

[25] H. Kim, J. Lu, M.S. Sacks, K.B. Chandran, Dynamic simulation of bioprosthetic heart valves using a stress resultant shell model, Ann. Biomed. Eng. 36 (2008) 262–275.

[26] K.S. Kunzelman, R.P. Cochran, C. Chuong, W.S. Ring, E.D. Verrier, R.D. Eberhart, Finite element analysis of the mitral valve., J. Heart Valve Dis. 2 (1993) 326–340.

[27] K.S. Kunzelman, D.W. Quick, R.P. Cochran, Altered collagen concentration in mitral valve leaflets: biochemical and finite element analysis, Ann. Thorac. Surg.

66 (1998) S198–S205.

[28] W. Sun, M.S. Sacks, T.L. Sellaro, W.S. Slaughter, M.J. Scott, Biaxial mechanical response of bioprosthetic heart valve biomaterials to high in-plane shear, J. Biomech. Eng. 125 (2003) 372–380.

[29] P.E. Hammer, M.S. Sacks, P.J. Del Nido, R.D. Howe, Mass-spring model for simulation of heart valve tissue mechanical behavior, Ann. Biomed. Eng. 39 (2011) 1668–1679.

[30] R.L. Taylor, E. Onate, P.-A. Ubach, Finite element analysis of membrane structures, Springer, 2005.

[31] M. Abbasi, A.N. Azadani, Leaflet stress and strain distributions following incomplete transcatheter aortic valve expansion, J. Biomech. 48 (2015) 3663–3671.

[32] M.S. Sacks, Biaxial mechanical evaluation of planar biological materials, J. Elast. Phys. Sci. Solids. 61 (2000) 199–246.

[33] W. Sun, A. Abad, M.S. Sacks, Simulated bioprosthetic heart valve deformation under quasi-static loading, (2005).

[34] G.A. Holzapfel, R.W. Ogden, On planar biaxial tests for anisotropic nonlinearly elastic solids. A continuum mechanical framework, Math. Mech. Solids. 14 (2009) 474–489.

[35] E.D. Hiester, M.S. Sacks, Optimal bovine pericardial tissue selection sites. I. Fiber architecture and tissue thickness measurements, J. Biomed. Mater. Res. An Off. J. Soc. Biomater. Japanese Soc. Biomater. Aust. Soc. Biomater. 39 (1998) 207–214.

[36] I. Borazjani, A review of fluid-structure interaction simulations of prosthetic heart valves, J. Long. Term. Eff. Med. Implants. 25 (2015).

[37] C. Andersson, D. Ahl, Fluid structure interaction: Evaluation of two coupling techniques, (2011).

[38] C. Förster, W.A. Wall, E. Ramm, Artificial added mass instabilities in sequential staggered coupling of nonlinear structures and incompressible viscous flows, Comput. Methods Appl. Mech. Eng. 196 (2007) 1278–1293.

[39] J. Donea, S. Giuliani, J.-P. Halleux, An arbitrary Lagrangian-Eulerian finite element method for transient dynamic fluid-structure interactions, Comput. Methods Appl. Mech. Eng. 33 (1982) 689–723.

[40] C.S. Peskin, Flow patterns around heart valves: A numerical method, J. Comput. Phys. 10 (1972) 252–271. https://doi.org/https://doi.org/10.1016/0021-9991(72)90065-4.

[41] R. Mittal, G. Iaccarino, Immersed boundary methods, Annu. Rev. Fluid Mech. 37

(2005) 239–261.

[42] C.S. Peskin, D.M. McQueen, A three-dimensional computational method for blood flow in the heart I. Immersed elastic fibers in a viscous incompressible fluid, J. Comput. Phys. 81 (1989) 372–405.

[43] C.S. Peskin, Numerical analysis of blood flow in the heart, J. Comput. Phys. 25 (1977) 220–252.

[44] B.E. Griffith, R.D. Hornung, D.M. McQueen, C.S. Peskin, An adaptive, formally second order accurate version of the immersed boundary method, J. Comput. Phys. 223 (2007) 10–49.

[45] D.M. Espino, D.E.T. Shepherd, D.W.L. Hukins, Evaluation of a transient, simultaneous, arbitrary Lagrange–Euler based multi-physics method for simulating the mitral heart valve, Comput. Methods Biomech. Biomed. Engin. 17 (2014) 450–458.

[46] L. Cai, Y. Hao, P. Ma, G. Zhu, X. Luo, H. Gao, Fluid-structure interaction simulation of calcified aortic valve stenosis, Math. Biosci. Eng. (2022).

[47] M.-C. Hsu, D. Kamensky, Y. Bazilevs, M.S. Sacks, T.J.R. Hughes, Fluid–structure interaction analysis of bioprosthetic heart valves: significance of arterial wall deformation, Comput. Mech. 54 (2014) 1055–1071.

[48] Advantage of commercial software 1, (n.d.) https://www.braveriver.com/blog/benefits-of-open-s.

[49] Advantege 2, (n.d.). https://www.codecreators.ca/custom-software-vs-commercial-software-need-know/#:~:text=Advantages of commercial Software development&text=There is no need to spend time in the development process.&text=Support%2C maintenance services and help,users are usi.

[50] A. Fedeli, C. Montecucco, G.L. Gragnani, Open-source software for electromagnetic scattering simulation: The case of antenna design, Electronics. 8 (2019) 1506.

[51] advantage 4, (n.d.). https://www.toppr.com/guides/computer-science/computer-fundamentals/open-source-concepts/proprietary-software/#Advantages_of_Proprietary_Software.

[52] Advantage 6, (n.d.). https://eomag.eu/10-differences-between-commercial-and-open-source-gis-software/#:~:text=Open-source software is computer,inspect%2C change and enhance it.

[53] H. Mohammadi, K. Mequanint, Prosthetic aortic heart valves: modeling and design, Med. Eng. Phys. 33 (2011) 131–147.

[54] F.J. Schoen, Evolving concepts of cardiac valve dynamics: the continuum of development, functional structure, pathobiology, and tissue engineering,

Circulation. 118 (2008) 1864–1880.

[55] H. Tam, W. Zhang, D. Infante, N. Parchment, M. Sacks, N. Vyavahare, Fixation of bovine pericardium-based tissue biomaterial with irreversible chemistry improves biochemical and biomechanical properties, J. Cardiovasc. Transl. Res. 10 (2017) 194–205.

[56] G. Goissis, A. de Fátima Giglioti, D.M. Braile, Preparation and characterization of an acellular bovine pericardium intended for manufacture of valve bioprostheses, Artif. Organs. 35 (2011) 484–489.

[57] P. Singhal, A. Luk, J. Butany, Bioprosthetic heart valves: impact of implantation on biomaterials, Int. Sch. Res. Not. 2013 (2013).

[58] B. Meuris, H. De Praetere, M. Strasly, P. Trabucco, J.C. Lai, P. Verbrugghe, P. Herijgers, A novel tissue treatment to reduce mineralization of bovine pericardial heart valves, J. Thorac. Cardiovasc. Surg. 156 (2018) 197–206.

[59] C.M. Cunanan, C.M. Cabiling, T.T. Dinh, S. Shen, P. Tran-Hata, J.H. Rutledge III, M.C. Fishbein, Tissue characterization and calcification potential of commercial bioprosthetic heart valves, Ann. Thorac. Surg. 71 (2001) S417–S421.

[60] J. Dove, M. Howanec, M. Thubrikar, Carpentier-Edwards ThermaFix Process: a method for extracting calcium binding sites from pericardial tissue, Edwards Lifesciences LLC. (2006).

[61] W. Flameng, H. Hermans, E. Verbeken, B. Meuris, A randomized assessment of an advanced tissue preservation technology in the juvenile sheep model, J. Thorac. Cardiovasc. Surg. 149 (2015) 340–345.

[62] J.D. Puskas, J.E. Bavaria, L.G. Svensson, E.H. Blackstone, B. Griffith, J.S. Gammie, D.A. Heimansohn, J. Sadowski, K. Bartus, D.R. Johnston, The COMMENCE trial: 2-year outcomes with an aortic bioprosthesis with RESILIA tissue, Eur. J. Cardio-Thoracic Surg. 52 (2017) 432–439.

[63] D.R. Johnston, B.P. Griffith, J.D. Puskas, J.E. Bavaria, L.G. Svensson, E.H. Blackstone, J.S. Gammie, D.A. Heimansohn, J. Sadowski, K. Bartus, Intermediate-term outcomes of aortic valve replacement using a bioprosthesis with a novel tissue, J. Thorac. Cardiovasc. Surg. 162 (2021) 1478–1485.

[64] E.D. Hiester, M.S. Sacks, Optimal bovine pericardial tissue selection sites. II. Cartographic analysis, J. Biomed. Mater. Res. An Off. J. Soc. Biomater. Japanese Soc. Biomater. Aust. Soc. Biomater. 39 (1998) 215–221.

[65] M.S. Sacks, A. Mirnajafi, W. Sun, P. Schmidt, Bioprosthetic heart valve heterograft biomaterials: structure, mechanical behavior and computational simulation, Expert Rev. Med. Devices. 3 (2006) 817–834.

[66] M. Abbasi, M.S. Barakat, K. Vahidkhah, A.N. Azadani, Characterization of three-dimensional anisotropic heart valve tissue mechanical properties using inverse

finite element analysis, J. Mech. Behav. Biomed. Mater. 62 (2016) 33–44.

[67] I. Borazjani, Fluid–structure interaction, immersed boundary-finite element method simulations of bio-prosthetic heart valves, Comput. Methods Appl. Mech. Eng. 257 (2013) 103–116.

[68] P.N. Jermihov, L. Jia, M.S. Sacks, R.C. Gorman, J.H. Gorman, K.B. Chandran, Effect of geometry on the leaflet stresses in simulated models of congenital bicuspid aortic valves, Cardiovasc. Eng. Technol. 2 (2011) 48–56.

[69] Edwards. Edwards bovine pericardial patch. https://, (n.d.). /www.edwards.com/devices/bovinepericardial-patches/cardiac.

[70] G.P. Association, Physical properties of glycerine and its solutions, Glycerine Producers' Association, 1963.

[71] M. Abbasi, M.S. Barakat, D. Dvir, A.N. Azadani, A non-invasive material characterization framework for bioprosthetic heart valves, Ann. Biomed. Eng. 47 (2019) 97–112.

[72] H. Kim, J. Lu, M.S. Sacks, K.B. Chandran, Dynamic simulation pericardial bioprosthetic heart valve function, (2006).

[73] E.L. Johnson, M.C.H. Wu, F. Xu, N.M. Wiese, M.R. Rajanna, A.J. Herrema, B. Ganapathysubramanian, T.J.R. Hughes, M.S. Sacks, M.-C. Hsu, Thinner biological tissues induce leaflet flutter in aortic heart valve replacements, Proc. Natl. Acad. Sci. 117 (2020) 19007–19016.

[74] M.E.P. Goad, D.L. Goad, Biomedical materials and devices, in: Haschek Rousseaux's Handb. Toxicol. Pathol., Elsevier, 2013: pp. 783–806.

[75] W.M. Haschek, C.G. Rousseaux, M.A. Wallig, B. Bolon, Haschek and Rousseaux's Handbook of Toxicologic Pathology, Volume 1: Principles and Practice of Toxicologic Pathology, Academic Press, 2021.

[76] N. Vyavahare, M. Ogle, F.J. Schoen, R. Zand, D.C. Gloeckner, M. Sacks, R.J. Levy, Mechanisms of bioprosthetic heart valve failure: fatigue causes collagen denaturation and glycosaminoglycan loss, J. Biomed. Mater. Res. An Off. J. Soc. Biomater. Japanese Soc. Biomater. Aust. Soc. Biomater. 46 (1999) 44–50.

[77] M.S. Sacks, W.D. Merryman, D.E. Schmidt, On the biomechanics of heart valve function, J. Biomech. 42 (2009) 1804–1824.

[78] A.E. Kostyunin, A.E. Yuzhalin, M.A. Rezvova, E.A. Ovcharenko, T. V Glushkova, A.G. Kutikhin, Degeneration of bioprosthetic heart valves: update 2020, J. Am. Heart Assoc. 9 (2020) e018506.

[79] M. Barakat, D. Dvir, A.N. Azadani, Fluid dynamic characterization of transcatheter aortic valves using particle image velocimetry, Artif. Organs. 42 (2018) E357–E368.

[80] L.P. Dasi, H.A. Simon, P. Sucosky, A.P. Yoganathan, Fluid mechanics of artificial heart valves, Clin. Exp. Pharmacol. Physiol. 36 (2009) 225–237.

[81] A.P. Yoganathan, Z. He, S. Casey Jones, Fluid mechanics of heart valves, Annu. Rev. Biomed. Eng. 6 (2004) 331–362.

[82] R.C. Becker, P. Eisenberg, A.G.G. Turpie, Pathobiologic features and prevention of thrombotic complications associated with prosthetic heart valves: fundamental principles and the contribution of platelets and thrombin, Am. Heart J. 141 (2001) 1025–1037.

[83] L.B. Leverett, J.D. Hellums, C.P. Alfrey, E.C. Lynch, Red blood cell damage by shear stress, Biophys. J. 12 (1972) 257–273.

[84] S.F.C. Stewart, E.G. Paterson, G.W. Burgreen, P. Hariharan, M. Giarra, V. Reddy, S.W. Day, K.B. Manning, S. Deutsch, M.R. Berman, Assessment of CFD performance in simulations of an idealized medical device: results of FDA's first computational interlaboratory study, Cardiovasc. Eng. Technol. 3 (2012) 139–160.

[85] P.D. Morris, A. Narracott, H. von Tengg-Kobligk, D.A.S. Soto, S. Hsiao, A. Lungu, P. Evans, N.W. Bressloff, P. V Lawford, D.R. Hose, Computational fluid dynamics modelling in cardiovascular medicine, Heart. 102 (2016) 18–28.

[86] H.A. Dwyer, P.B. Matthews, A. Azadani, N. Jaussaud, L. Ge, T.S. Guy, E.E. Tseng, Computational fluid dynamics simulation of transcatheter aortic valve degeneration, Interact. Cardiovasc. Thorac. Surg. 9 (2009) 301–308.

[87] E. Sirois, W. Sun, Computational evaluation of platelet activation induced by a bioprosthetic heart valve, Artif. Organs. 35 (2011) 157–165.

[88] E. De Marchena, J. Mesa, S. Pomenti, C. Marin y Kall, X. Marincic, K. Yahagi, E. Ladich, R. Kutys, Y. Aga, M. Ragosta, Thrombus formation following transcatheter aortic valve replacement, JACC Cardiovasc. Interv. 8 (2015) 728–739.

[89] Lee, J.H., Rygg, A.D., Kolahdouz, E.M., Rossi, S., Retta, S.M., Duraiswamy, N., Scotten, L.N., Craven, B.A. and Griffith, B.E., Fluid–structure interaction models of bioprosthetic heart valve dynamics in an experimental pulse duplicator, Annals of biomedical engineering. 48 (2020) 1475-1490.